This manuscript was accepted by J. Chem. Phys. Click here to see the version of record.

Transport properties of the binary mixtures of the three organic liquids toluene, methanol and cyclohexane

E.Lapeira,[1] M. Gebhardt,[2] T. Triller,[2] A.Mialdun,[3] W. Köhler,[2, a)] V. Shevtsova,[3, b)] and M. M. Bou-Ali[1, c)]

[1)] *Mech. and Manufacturing Dept, MGEP Mondragon Goi Eskola Politeknikoa, Loramendi 4 Apdo. 23, 20500 Mondragon, Spain*

[2)] *Physikalisches Institut, Universität Bayreuth, D-95440 Bayreuth, Germany*

[3)] *MRC, CP165/62, Université Libre de Bruxelles, Av. F.D. Roosevelt, 50, B-1050, Brussels, Belgium*

We report on the measurements of diffusion (D), thermodiffusion (D_T) and Soret (S_T) coefficients in binary pairs of the ternary system toluene-methanol-cyclohexane using different instrumental techniques: microgravity measurements (SODI/DCMIX2) on the International Space Station (ISS), thermogravitational column (TGC) in combination with sliding symmetric tubes (SST), optical beam deflection (OBD), optical digital interferometry (ODI) and Counter Flow Cell (CFC). The binary systems have large regions where the mixtures are either not miscible or the Soret coefficient is negative. All the coefficients have been measured over a wide composition range with the exception of a miscibility gap. Results from different instruments and literature data are in favorable agreement over a broad composition range. Additionally, we have carefully measured the physical properties and the optical contrast factors $(\partial n/\partial c)_{p,T}$ and $(\partial n/\partial T)_{p,c}$. The latter ones were also calculated using the Looyenga equation. The measurements in methanol-cyclohexane mixture revealed a decay of the diffusion coefficient when approaching the miscibility gap. We have interpreted this in the spirit of the pseudospinodal concept.

Keywords: diffusion, thermodiffusion, Soret effect, spinodal

[a)] Electronic mail: werner.koehler@uni-bayreuth.de

[b)] Electronic mail: vshev@ulb.ac.be

[c)] Electronic mail: mbouali@mondragon.edu

I. INTRODUCTION

The mass transport caused by a temperature gradient influences many properties and processes in multicomponent systems. During recent years, the focus of research on these transport mechanisms, which is known as thermodiffusion, thermal diffusion or the Soret effect, has been extended from binary to ternary mixtures, which are significantly more difficult to examine[1,2]. Besides the purely scientific interest in the underlying mechanisms, research is motivated by a number of phenomena of practical relevance. The prediction of mass transfer processes in systems of industrial interest greatly relies on the knowledge of the diffusion and thermodiffusion coefficients, which appear in the equations modeling these phenomena. Recently, several techniques have been developed for the measurement of diffusion and thermodiffusion coefficients in ternary fluid mixtures. Other than for binary mixtures, where reliable measurements are done on a routine basis, the results reported so far for ternary mixtures do not provide consistent estimates of the Soret[3–6] and diffusion[3,7–9] coefficients. There are subtle issues in connections with experimental and mathematical challenges. Beside, in the laboratory tests even in theoretically stable configurations convection could appear due to the non-ideality of the experimental setup.

Microgravity conditions provide an ideal environment for the investigation of transport processes in the absence of convection. Mass diffusion effects are typically slow and require long microgravity time, which can be offered only by the International Space Station (ISS). There, thermodiffusion experiments can be conducted inside the SODI (Selected Optical Diagnostic Instrument) instrument in binary[10] and ternary mixtures[11] by using both one- and two-color interferometry.

In the framework of the DCMIX (Diffusion Coefficients in MIXtures) project, measurements onboard the ISS have already been performed for two ternary systems in course of the DCMIX$_1$ and the DCMIX$_2$ campaigns. In DCMIX$_1$, hydrocarbons (tetralin, isobutylbenzene, and n-dodecane, THN-IBB-C12) [6,12] and in DCMIX$_2$, a ternary mixture with a miscibility gap [13,14], a consolute critical point, and a large composition range with negative Soret coefficients (toluene-methanol-cyclohexane, Tol-Meth-Ch) have been studied.

One composition of the DCMIX$_1$ mixtures, THN/IBB/C12 with 0.8/0.1/0.1 mass fractions, was selected for a benchmark campaign[6]. The choice of this particular composition resulted from the requirement of an acceptable condition number of the contrast factor matrix. The benchmark results once again demonstrated that the extraction of six independent parameters from the measured signals, i.e., two Soret and four diffusion coefficients, is by no means straightforward. In order to perform a systematic study of a ternary mixture, in particular the precise knowledge of the coefficients along the binary limits is important. For the DCMIX$_1$ system THN-IBB-C12, a study of the binary limits has recently been reported[15]. Here, we present the corresponding study for the binary mixtures of the DCMIX$_2$ system Tol-Meth-Ch.

The data presented in this work cover a wide range of compositions as shown in Fig.1.

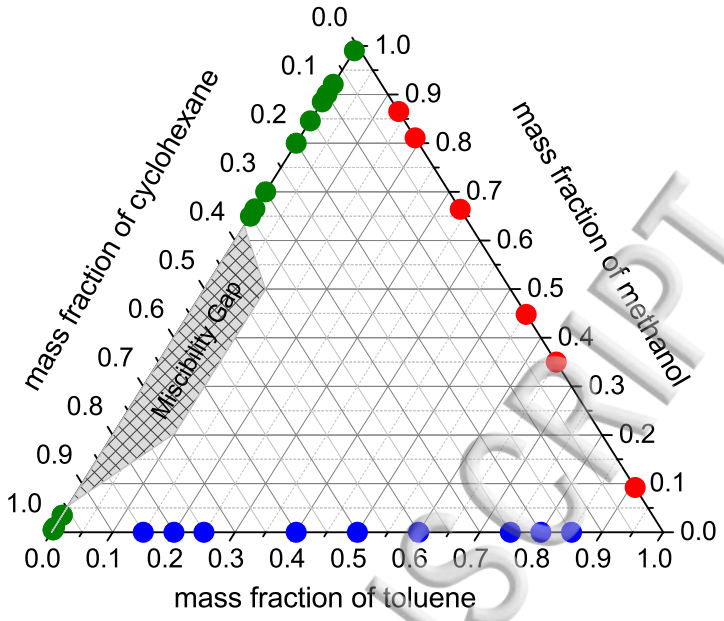

FIG. 1. Map of Toluene-Methanol-Cyclohexane mixture in mass fractions. The symbols indicate the compositions for which transport coefficients have been measured

They have been measured on ground by different techniques in the participating laboratories. The coefficients of one particular composition (Tol/Ch–0.4/0.6) were measured in the $DCMIX_2$ experiment onboard the ISS at different mean temperatures[14]. The experimental techniques employed by the three participating laboratories are the thermogravitational column (TGC) and the sliding symmetric tubes (SST) technique (UM, University of Mondragon, Spain); optical beam deflection (OBD) (UB, University of Bayreuth, Germany); optical digital interferometry (ODI) and counter flow cell (CFC) (ULB, University of Brussels, Belgium). The experimental technique used in the microgravity experiment $DCMIX_2$ is similar but not identical to the ODI technique developed in Brussels. The number of inputs from the various methods is different as the systems with negative Soret coefficient could only be measured by OBD and on the ISS. The physical properties of the mixtures such as density, viscosity, refractive indices, and contrast factors were measured in addition to the transport properties of the mixtures. The complete set of reliable data will also provide a valuable contribution for the research aimed at hydrodynamic or double-diffusive instability in these mixtures.

This paper is organized as follows: Section II presents a short description of all employed experimental techniques. Section III reports on the results and discussion of the measurements of contracts factors and transport coefficients and the comparison with literature data. Finally, the conclusions are drawn in Section IV.

III. EXPERIMENTAL TECHNIQUES

Among the set-ups employed in this study only the SODI instrument in the DCMIX-configuration for the binary mixture has not yet been presented. The previously used ground experiments will only briefly be described and details can be found elsewhere[16]. We begin our description with the SODI instrument and compare it to the ODI set-up used on ground.

A. Optical digital interferometry (ODI): the microgravity and laboratory instruments

A unique feature of the ODI method is that it traces the *transient* path of the system over the *entire* two-dimensional cross section of the cell. In the set-up on the ISS, five Soret cells with ternary mixtures of different compositions (primary cells) and one cell with the reference binary mixture (companion cell) are integrated into a one-piece structure, which is called the cell array. All cells are identical, they are transparent with inner dimensions of $L_{\mu g} \times W_{\mu g} \times H_{\mu g} = 10 \times 10 \times 5$ mm^3. Here L is the path that the beam passes through in the liquid volume, W is the wideness of the cell and H is the diffusion path, i.e., the distance between the working surfaces of the plates; the subscript μg stands for microgravity. The glass frame is clamped from the top and the bottom in between two copper blocks that are thermally stabilized by Peltier elements, which maintain a temperature gradient across the cell. The cross-section of a cell is shown in Fig. 2(a). The cell array is part of the SODI instrument which is equipped with a two-wavelength (670 nm and 935 nm) Mach-Zehnder interferometer to spatially resolve the concentration distribution within the cell. In the DCMIX$_2$ experiment, the binary cell is filled with the mixture Tol/Ch (0.4/0.6), for which only a red laser diode emitting at $\lambda = 670$ nm wavelength is used. In total 11 experimental runs were conducted in the binary cell at different mean temperatures ranging from 293.15 K up to 307.15 K. The temperature difference applied across the cell was $\Delta T = 5$ K (i.e. 1 K/mm) with a typical stability of ± 0.02 K. The resolution of the imaging system is about 150 pixels/mm.

A laboratory setup for the measurement of the Soret effect by optical digital interferometry (ODI) has been developed at ULB[17,18]. The cell has inner dimensions of $L_g \times W_g \times H_g = 18 \times 18 \times 6.06$ mm^3 (the subscript g means ground laboratory) and is custom made from optical quality fused silica with a wall thickness of 2 mm. Similarly to the microgravity cell, a rectangular glass frame is clamped between two nickel-plated copper blocks with special indium seals. The use of these seals allows to avoid problems from lateral heat fluxes in the experimental cell. The cross-section of one cell is shown in Fig. 2(b). Each copper block is thermostabilized by Peltier elements driven independently by PID controllers, which allow for a temperature stability of ± 0.002 K. The temperature gradient applied across the cell was close to 1 K/mm in all measurements.

In spite of the same type of probing (Mach-Zehnder interferometer), the instruments have

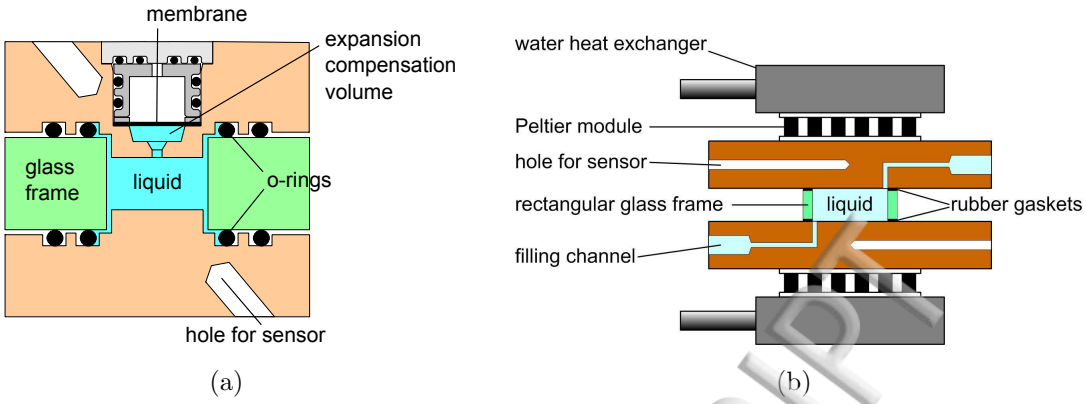

FIG. 2. (a) Cross-section of the cell used in microgravity. (b) Cross-section of the cell used in the laboratory.

many specific features. In the SODI instrument, a phase-shifting technique is employed to determine the phase difference between the probe and the reference beam using five successive fringe images. Each image is acquired at a particular value of the laser diode driving current. The stepwise variation of the laser current provides the wavelength shift and, consequently, the optical phase shift between subsequent interferograms of the stack. The typical time lag between the last and first interference patterns within a stack does not exceed 1 s, and it has no effect in a slow diffusion-controlled process. To obtain the optical phase from the stack of interferograms we have used a modified version of Hariharan's algorithm[19]. The expression for the phase evaluation is

$$\varphi(x,z) = \arctan \frac{7(I_4 - I_2)}{4I_1 - I_2 - 6I_3 - I_4 + 4I_5} \ . \tag{1}$$

The spatial coordinates of the image intensities $I_i(x,z)$ have been omitted for clarity. For this technique the interferometer is adjusted to provide wide fringes. An example of an optical phase is shown in Fig. 3(a).

In order to reconstruct a spatial distribution of the optical phase in the ground set-up, the Fourier transform method is applied. The phase distribution is obtained from two different interferograms as the interference pattern of interest is always processed against a reference interferogram taken before the refractive index change. The interferometer is adjusted to provide a narrow fringe pattern and obtained phase map is shown in Fig. 3(b).

A comparison of the optical phases in Fig. 3 reveals a strong perturbation of the isolines linearity in the upper part of the microgravity cell. There are a few reasons for this. SODI is a multi-user instrument, and the test cell has specific design features (see Fig. 2(a)). To facilitate the observation of the entire liquid volume, the copper blocks have protrusions that enter the opening in the glass frame by approximately 2 mm. Furthermore, due to the double-containment requirement (i.e., leakage-preventing barrier), there are two rubber O-rings between the glass frame and each copper block. The blocks, in turn, contain grooves to accommodate these seals. This cell geometry leads to a deviation of the temperature

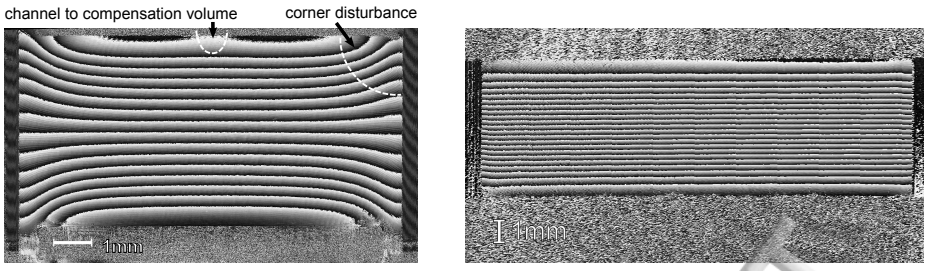

FIG. 3. Wrapped phase map after subtraction of the reference image obtained with the red laser, which corresponds to the end of the Soret separation phase: (a) microgravity and (b) ground set-ups, respectively.

field from linearity along the vertical direction, particularly near the corners of the cell. To resolve the problem of non-linearity in the corners, a tomographic reconstruction of the 3D concentration distribution has recently been suggested[20].

Another feature of the cell design that affects the thermodiffusion separation process is a compensation volume for thermal expansion. This forms a *dead* volume with a nearly isothermal liquid. It is not directly involved in the Soret separation, but it perturbs the separation by diffusive mass exchange with neighboring regions already affected by thermodiffusion. It can be seen from the distortion of the upper fringe at the central part of the cell in Fig. 3(a). To resolve the problem of the compensation volume, it is suggested to take only the variation of the refractive index in the lower half into account. After this, the data extraction procedure from the wrapped phase images is practically identical for the microgravity and the ground experiments.

The quantity obtained after processing an interferogram is a spatial phase distribution $\Delta\varphi(x,z,t)$, which is transferred into a concentration distribution by the equation

$$\frac{\lambda}{2\,\pi\,L}\Delta\varphi(x,z,t) = \left(\frac{\partial n}{\partial c}\right)_{p,T} \Delta c(x,z,t) + \left(\frac{\partial n}{\partial T}\right)_{p,c} \Delta T(x,z,t)\ . \qquad (2)$$

The second term is defined during the initial step of the experiment[18]. Consequently, Soret and diffusion coefficients are simultaneously extracted by fitting of $\Delta c(x,z,t)$ from Eq. (2), averaged in x-direction, with the 1-D analytical solution

$$c(z,t) = c_0 + c_0(1-c_0)\,S_T\Delta T\left[\frac{1}{2} - \frac{z}{H} - \frac{4}{\pi^2}\sum_{n,odd}^{\infty}\frac{1}{n^2}\cos\left(\frac{n\pi z}{H}\right)\exp\left(-\frac{n^2\pi^2}{H^2}D\,t\right)\right]. \qquad (3)$$

B. Counter Flow Cell (CFC)

Isothermal mass diffusion measurements at ULB were conducted by the counter flow method for creating an interface between two solutions of different but close concentrations ($\Delta c = 0.01$ in most cases). At the beginning of each experimental run, a two-layer liquid

system is formed inside the diffusion cell of 20 mm height by the simultaneous injection of two solutions through the inlets, heavier mixture from bottom and lighter one from top. The excess of liquid leaves the cell through the orifices located in the side walls at the level of the interface, i.e., 10 mm from the bottom. This cell design allows to create a steep initial concentration drop between the two layers in the thickness range of about 0.3 mm.

To examine the change in the refractive index of liquid within the cell, the classical Mach-Zehnder interferometer scheme was used. The light source is an expanded and collimated beam of a laser diode emitting at $\lambda = 670\,\mathrm{nm}$. More than 200 interferograms are acquired by 1.2 mega-pixel CCD camera during typical experiment time of 10 h. Optical phase information is extracted from the fringe images by 2-D Fourier transform technique[18].

The whole set-up, including the cell, was maintained inside a thermally insulated box equipped with a system of active thermal regulation. The temperature inside the box was kept at 298.15 K with residual fluctuations of less than ± 0.1 K. Detailed description of similar cell and a data extraction procedure can be found elsewhere[7].

C. Thermogravitational column (TGC) & Sliding Symmetric Tubes (SST)

Two different instruments were used at UM: the thermogravitational column (TGC) and sliding symmetric tubes (SST) for measurements of thermodiffusion and mass diffusion coefficients, respectively. The employed plane thermogravitational column [21] is characterized by the following parameters: a plane-parallel column has a length of $L_z = (98.0 \pm 0.1)\,\mathrm{cm}$, gap dimension $L_x = (0.102 \pm 0.0005)\,\mathrm{cm}$, and width $L_y = (5.0 \pm 0.1)\,\mathrm{cm}$. In the column, a mixture is placed in a narrow slot between two plates of different temperatures (Fig. 4). The horizontal temperature gradient imposed by heating (cooling) the walls induces horizontal composition gradients due to the Soret effect. It also results in convective flow driven by buoyancy forces. The flow is strictly vertical, except for the top and bottom ends of the slot. The horizontal separation of components in combination with the vertical convective current leads to an enhanced separation between the top and bottom ends. The theories for the column operation and for data extraction are well established. The vertical concentration gradient is given by[22,23]

$$\frac{\partial c}{\partial z} = -c_0\,(1 - c_0)\frac{504}{g\,L_x^4}\frac{D_T\,\nu}{\alpha}\,, \tag{4}$$

where x and z are the horizontal and vertical coordinates, ν is the kinematic viscosity of the mixture, α is the thermal expansion coefficient, and g is the gravity acceleration. Equation (4) is used to determine the thermodiffusion coefficient D_T from the concentration measurements along the column. Note that the separation in the column is independent of the temperature difference between the cold and hot plates.

The vertical concentration gradient is determined from the relation

$$dc/dz = (\beta_c\,\rho)^{-1}(d\rho/dz)\,. \tag{5}$$

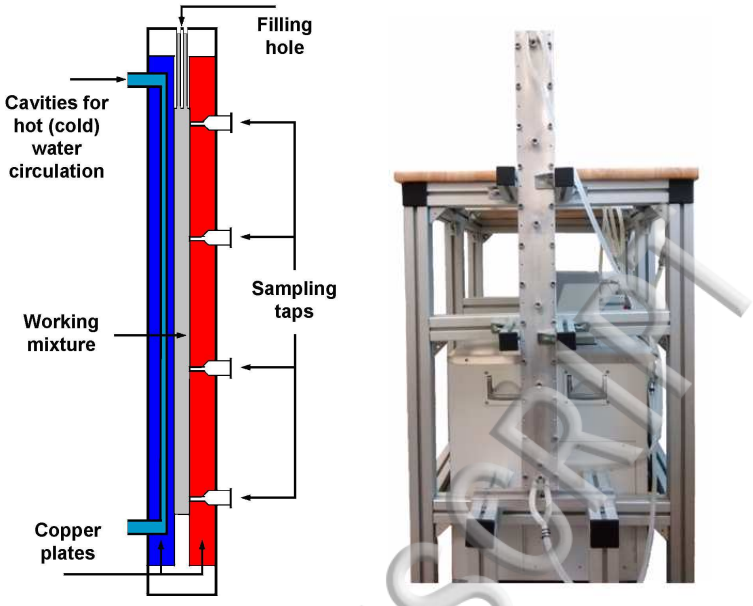

FIG. 4. Sketch of cross-section of thermogravitational column and image of real column.

The vertical density gradient along the column $d\rho/dz$ is directly obtained from the measurements of the density of five samples taken at evenly spaced elevations. In a narrow mass fraction range, the variation of ρ with height is linear. All the physical properties used in Eqs. (4)-(5) were measured prior to the experiments and they are presented below in Section III A.

The UM group has measured diffusion coefficients D using sliding symmetric tubes (SST)[9]. In this technique, two liquid mixtures ($c_{0,up}$, $c_{0,low}$) with slightly different concentrations around the point of interest ($c_0 \pm 3\%$) are placed into two tubular containers (subscripts *up* and *low* stand for upper and lower). In the experiment, typically 10 sets of such two-tube cells, with the same initial concentration of the mixtures are used (see Fig. 5). To prevent convection, the mixture with the higher concentration of the denser component is placed in the lower tube. The sets are then introduced into a water bath and given time to equilibrate at the working temperature, which is controlled with a precision of 0.1K (Fig. 5). All pairs of tubes are then simultaneously brought into contact with each other and the diffusion process starts. From this point on, the initial concentration difference between the corresponding tubes gradually decreases by diffusion. Separating different pairs of tubes, one by one with a certain time step, the mean concentrations in the upper and lower parts $\overline{c_{up}}$, $\overline{c_{low}}$ are determined at successive moments of time. The diffusion coefficient is extracted from the slope of the concentration profile using the equation

$$S^{up} = \frac{(c_{low} - c_{up})}{L}\sqrt{\frac{D}{\pi}}\,. \tag{6}$$

where L is the length of the tube, S^{up} is the slope of the linear regression formed by the

concentration points in the upper tube.

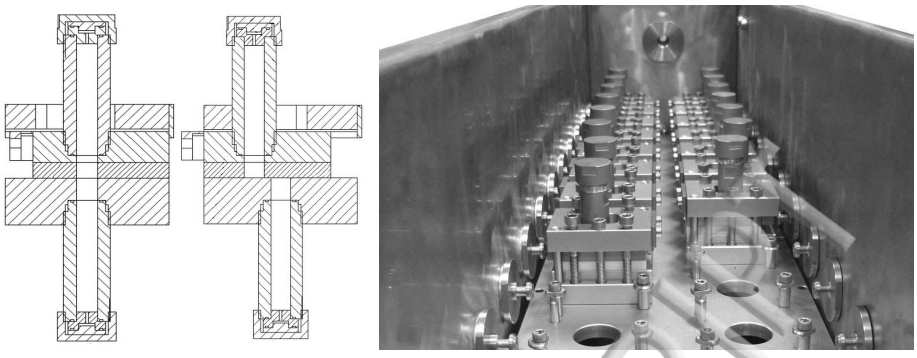

FIG. 5. Individual cell of sliding symmetric tubes instrument and the bath where the cells are introduced

D. Optical Beam Deflection

The experimental technique employed at UB is Optical Beam Deflection (OBD). The apparatus has already successfully been used to investigate binary thermodiffusion[24–26]. This particular setup is a single color version of the one described in Ref.[15] with a fiber coupled laser diode operating at a wavelength of 637 nm. The beam is coupled out from the fiber by means of a collimator, which is mounted on a profile rail together with the diffusion cell. The latter consists of two copper plates and a glass frame ($l = 1\,\mathrm{cm}$ geometric length, $h = 1.43\,\mathrm{mm}$ height) sandwiched in between. The temperature of either plate is controlled by Peltier elements and measured with thermistors. At the other end of the profile rail, at a distance of $l_d = 1.32\,\mathrm{m}$ from the diffusion cell, the beam displacement is detected by means of a line camera. The whole setup is housed inside an aluminum box in order to shield it from temperature and refractive index fluctuations of the air.

Application of a temperature gradient causes a refractive index gradient and a deflection δz of the laser beam:

$$\delta z = l\langle\frac{\partial n}{\partial z}\rangle\left(\frac{l}{2n} + \frac{l_\mathrm{w}}{n_\mathrm{w}} + \frac{l_\mathrm{d}}{n_\mathrm{air}}\right). \tag{7}$$

Here, n and n_{air} are the refractive indices of the sample and the air, respectively. The term l_w/n_w accounts for the contribution of the entrance and exit windows. The refractive index gradient

$$\frac{\partial n}{\partial z} = \left(\frac{\partial n}{\partial T}\right)_{p,c}\frac{\partial T}{\partial z} + \left(\frac{\partial n}{\partial c}\right)_{p,T}\frac{\partial c}{\partial z} \tag{8}$$

is averaged over the beam profile as suggested by Kolodner[27]. It results from the temperature and concentration gradients and the optical contrast factors $(\partial n/\partial T)_{p,c}$ and $(\partial n/\partial c)_{p,T}$. The transport coefficients are obtained from a fit to the measured beam deflection signal. The

temperature $T(t)$ and concentration $c(t)$ (mass fraction) are calculated as numerical solutions of the heat and extended diffusion equation

$$\partial_t T = D_{th} \Delta T \tag{9}$$

$$\partial_t c = D \Delta c + D_T c(1-c) \Delta T \tag{10}$$

using the measured temperatures of the copper plates as time-dependent boundary conditions.

In order to determine the optical contrast factors, the concentration and temperature dependence of the refractive index $n(c,T)$ was measured at $\lambda = 633$ nm by means of a refractometer (Anton Paar Abbemat WR-MW, $T = 293.15\,\mathrm{K}$) and an interferometer[28–30], respectively. Since the refractometer is only calibrated for $T = 293.15\,\mathrm{K}$, refractive indices at other temperatures, e.g. $T = 298.15\,\mathrm{K}$, are computed by integrating the interferometrically determined temperature derivative $(\partial n/\partial T)_{p,c}$. The slight difference between the wavelength used to measure the contrast factors (633 nm) and the one employed for OBD (637 nm) has been neglected. The density of the samples was measured with an commercial density meter (Anton Paar, DSA 5000). All samples were prepared using a precision balance (Sartorius, BP211D).

III. RESULTS AND DISCUSSION

A. Physical properties

The sign of the Soret coefficient in all binary subsystems is negative in a large concentration region, if not everywhere. It turns the mixture into an attractive system for the theoretical and numerical analysis because it can lead to instabilities in a non-uniform temperature field in the presence of gravity. These studies require knowledge of all relevant physical properties of the system, including viscosity, thermal and mass expansion coefficients, and density. Thus, we have measured these properties along with diffusion and Soret coefficients in order to provide all necessary information for theoretical studies of this system and their comparison with experimental observations. Furthermore, the determination of the thermodiffusion coefficient by the thermogravitational technique (Eq. (4)) requires knowledge of thermophysical properties of the mixture such as dynamic viscosity, thermal expansion coefficient, mass expansion coefficient, and density. These properties measured at UM are summarized in Table I. All the chemicals used were purchased from Merck with a purity of better than 99%.

An Anton Paar DMA 5000 vibrating quartz U-tube densimeter with a precision of $1 \cdot 10^{-6}\,\mathrm{g/cm^3}$ and an accuracy of $5 \cdot 10^{-6}\,\mathrm{g/cm^3}$ has been used to determine the density of the extracted samples along the column and the initial density of the sample. The thermal expansion coefficient α of the mixture was obtained from a linear fit to the density of the

TABLE I. Physical properties of the binary mixtures measured at $T = 298.15\,\mathrm{K}$: density ρ, viscosity μ, thermal expansion $\alpha = -\rho^{-1}\partial\rho/\partial T$ and solutal expansion $\beta = \rho^{-1}\partial\rho/\partial c$.

c_1 mass frac.	ρ kg/m^3	μ mPa·s	$\alpha/10^{-3}$ K^{-1}	$\beta/10^{-2}$
	Toluene (1) + Methanol (2)			
0.000	786.608	0.544	1.199	
0.135	796.498	0.557	1.194	9.26
0.189	800.495	0.562	1.189	9.23
0.336	811.444	0.572	1.181	9.16
0.552	827.632	0.578	1.160	9.10
0.650	835.055	0.571	1.150	9.09
0.908	854.772	0.545	1.113	9.09
1.000	862.179	0.552	1.082	
	Toluene (1) + Cyclohexane (2)			
0.00	773.852	0.893	1.220	
0.20	787.146	0.727	1.198	9.16
0.40	802.661	0.632	1.168	10.40
0.50	811.274	0.602	1.154	10.96
0.60	820.385	0.578	1.139	11.52
0.80	840.222	0.557	1.109	12.39
1.00	862.179	0.552	1.082	
	Methanol (1) + Cyclohexane (2)			
0.00	773.852	0.893	1.220	
0.03	772.648	0.842	1.245	-3.21
0.70	775.559	0.595	1.241	3.04
0.75	776.882	0.585	1.234	3.64
0.80	778.455	0.572	1.226	4.27
0.85	780.192	0.565	1.220	4.75
0.90	782.195	0.556	1.216	5.35
1.00	786.608	0.544	1.199	

fluid measured at five different temperatures between 297.15 and 299.15 K centered around the working temperature of $T = 298.15\,\mathrm{K}$. To determine the mass expansion coefficient β, the density of five samples at different concentrations around the working concentration has been measured. Both α and β, have been measured by means of the same Anton Paar DMA

5000.

A digital balance with a capacity of 310 g and accuracy of 0.0001 g has been used to prepare the mixtures and a manual falling ball Haake viscometer with an accuracy of better than 2% to determine their dynamic viscosity.

1. An approach for describing concentration dependence of physical properties.

One of the purposes of the study is to comprehensively characterise these three binary mixtures and to compare our data with those available in literature. All these binary mixtures have been extensively studied previously and we have collected in Table II the references where a property of at least one of them has been measured.

TABLE II. Literature sources of experimental binary mixture data on density ρ, dynamic viscosity μ and thermal expansion α at $T = 298.15\,\mathrm{K}$.

System		ρ	μ	α
Tol–Meth	All data	Refs.[31–35]	Refs.[31,33,34,36,37]	Ref.[31]
	Selected	Refs.[32,34]	Refs.[34,36]	—
Tol–Ch	All data	Refs.[38–42]	Refs.[40,42,43]	Refs.[38,42]
	Selected	Refs.[41,42]	Ref.[42]	Ref.[42]
Meth–Ch	All data	Ref.[44]	—	Ref.[45]
	Selected	Ref.[44]	—	—

[a] Data from Ref.[36] were obtained by extrapolation; data from Ref.[41] were obtained by correlation formula; data from Ref.[42] were obtained by interpolation; data on α from Refs.[31,38,42] were obtained by an analysis of $\rho(T)$ dependency; data on α in Ref.[45] were given for pure components only.

A careful analysis of the data provided by various authors has shown that they are of a very different quality. Thus, we first preselect the most reliable data and only then establish a correlation that accurately describes these data and our current results. It is rather difficult to distinguish between accurate and problematic data by a straightforward comparison of the measurements because for most of them the dependence on concentration is very close to a linear one. For this reason it is more informative to consider a deviation of the property from linear behavior (an analogue of 'excess' value) rather than the property itself.

This deviation from linearity of some property (e.g., density) $\Delta\rho$ is defined as

$$\Delta\rho = \rho^{\mathrm{exp}} - \rho^{\mathrm{lin}}, \quad \text{where} \quad \rho^{\mathrm{lin}} = \sum_{n=1}^{2} \rho_n^0 c_n = \rho_1^0 c_1 + \rho_2^0 (1 - c_1) = (\rho_1^0 - \rho_2^0) c_1 + \rho_2^0, \quad (11)$$

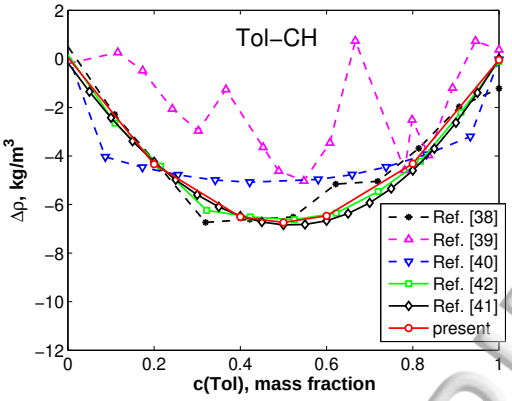

FIG. 6. Density deviation for Tol–CH binary system after[38–42] and as obtained in the present study.

here ρ_n^0 is the density of a pure n-th component, ρ^{lin} is the value of the density, linearly varying between ρ_1^0 and ρ_2^0 over the entire concentration range, c_1 is the mass fraction of component (1). There are several reasons for the use of density deviation despite the fact that in literature the most commonly used quantity is an excess molar volume. First, we prefer to stay within mass fractions as it is a directly measured quantity; second, the density correlation is used for deriving the solutal expansion coefficient.

All available literature data, recalculated to density deviation, are presented in Fig. 6. This example gives an idea about the criteria for the selection of good data. A quick inspection immediately shows which data have to be rejected from further consideration. The data by Pandey[39] have both high scattering and poor agreement by magnitude. The data by Iloukhani[40] moderately agree by magnitude, but display a very strange trend with high jumps at the extremes of the concentration span. The oldest data by Sanni[38] agree well by the average magnitude of $\Delta\rho$, but display noticeable scattering that also affects the extremities $c = 0$ and $c = 1$. Consequently, these three data-sets (shown by dashed curves in Fig. 6) have been rejected. Similar criteria have been applied to all other mixtures and properties. Accordingly, the complete list of the available data sources in Table II has been supplemented by the list of sources that have been selected for the use in the correlations. It is worth noting that for all the mixtures the data on density and dynamic viscosity are also available via REFPROP database[46]. We have found that this database provides acceptable rough estimates (up to a few percent discrepancy) but it fails when high precision is needed; in particular, it is unable to correctly reproduce even a sign of any deviation in property. It seems that the equations of state used in REFPROP are established using an outdated database.

The analysis of deviations is not only convenient for data comparison, but it is also useful for correlating/quantifying of dependencies as well. The drawback of this approach is that it requires an accurate definition of the properties of the pure components (anchor

points). Their accuracy has an additional importance since we intend to provide a consistent description of three binary subsystems of a ternary mixture; hence, the property of a pure component defined from two different binary mixtures should be the same. These reference values for pure components, determined by averaging the data from all preselected accurate data-sets and from this work, are listed in Table III. We do not provide the standard deviation for α in the table since mostly our data are available on this property.

TABLE III. Reference values of the physical properties of pure components at $T = 298.15\,\mathrm{K}$ obtained by averaging all the data from the selected sources listed in Table II and measured in this work.

	Units	Toluene	Methanol	Cyclohexane
ρ^0	kg/m^3	862.22 ± 0.07	786.63 ± 0.05	773.8 ± 0.13
$\mu^0\,/10^{-3}$	Pa·s	0.558 ± 0.006	0.547 ± 0.003	0.899 ± 0.010
$\alpha^0\,/10^{-3}$	K^{-1}	1.082	1.199	1.220

Usually polynomials of Redlich–Kister type[47] are used for the description of the excess properties and they are effective in accurate fitting of deviations.

$$\Delta\rho = c_1 c_2 \sum_{n=0}^{N} A_n (c_2 - c_1)^n = c_1(1-c_1) \sum_{n=0}^{N} A_n (1-2c_1)^n \,. \tag{12}$$

But since we are interested in the property itself, the Redlich–Kister excess polynomial is transformed into a classical power series polynomial. In most cases, the two terms in Eq. (12) provide an accurate description of the data. In a few particular cases, even one term might be enough, but for generality, a minimum of two terms are always used. Then, using Eqs. (11) and (12), the sought relation is written as

$$\begin{aligned} \rho = \rho^{\mathrm{lin}} + \Delta\rho \quad &= \rho_1^0 c_1 + \rho_2^0 (1-c_1) + c_1(1-c_1)\left[A_0 + A_1(1-2c_1)\right] \\ &= \rho_2^0 + (\rho_1^0 - \rho_2^0 + A_0 + A_1)c_1 + (-A_0 - 3A_1)c_1^2 + 2A_1 c_1^3 \,. \end{aligned} \tag{13}$$

To summarize, the approach describing the property is as follows. First, the deviation in property is calculated using Eq. (11) and the data for pure components from Table III. Then, Eq. (12) is fitted to this deviation, usually with two free parameters $\{A_0,\, A_1\}$. Finally, the Redlich–Kister polynomial for the deviation is transformed into a power series polynomial for the property using Eq. (13).

2. *Concentration dependence of physical properties: results.*

a. *Density and solutal expansion coefficient*

TABLE IV. Polynomial coefficients for correlation of density for three considered binary mixtures at $T = 298.15\,\mathrm{K}$.

	Units	Tol–Meth	Tol–CH	Meth–CH
Deviation in density, $\Delta\rho$				
A_0	$\mathrm{kg/m^3}$	−3.0884	−27.288	−37.390
A_1	$\mathrm{kg/m^3}$	0.7736	1.0620	−5.2931
Density, ρ				
d_0	$\mathrm{kg/m^3}$	786.63	773.80	773.80
d_1	$\mathrm{kg/m^3}$	73.275	62.194	−29.853
d_2	$\mathrm{kg/m^3}$	0.7677	24.102	53.269
d_3	$\mathrm{kg/m^3}$	1.5471	2.1240	−10.586
AAD_ρ	%	0.09	0.09	0.20
AAD_β	%	0.41	0.84	9.35

Using the above-described approach the density dependence on concentration is given by

$$\rho(c) = d_0 + d_1 \cdot c + d_2 \cdot c^2 + d_3 \cdot c^3\,, \tag{14}$$

where the concentration c is expressed in mass fraction of the first component of a binary pair. The coefficients d_i for the density of the studied mixtures are listed in Table IV. Additionally, we provided directly fitted coefficients of the Redlich–Kister type polynomial $\{A_0,\, A_1\}$. Figure 7 presents result of the fit for all binary mixtures.

Differentiation of the polynomial for ρ provides a reasonable description of the mass expansion coefficient β. Then, mass expansion can be calculated using the same polynomial coefficients as

$$\beta(c) = \frac{1}{\rho}\frac{\partial\rho}{\partial c} = \frac{d_1 + 2d_2 \cdot c + 3d_3 \cdot c^2}{d_0 + d_1 \cdot c + d_2 \cdot c^2 + d_3 \cdot c^3}\,. \tag{15}$$

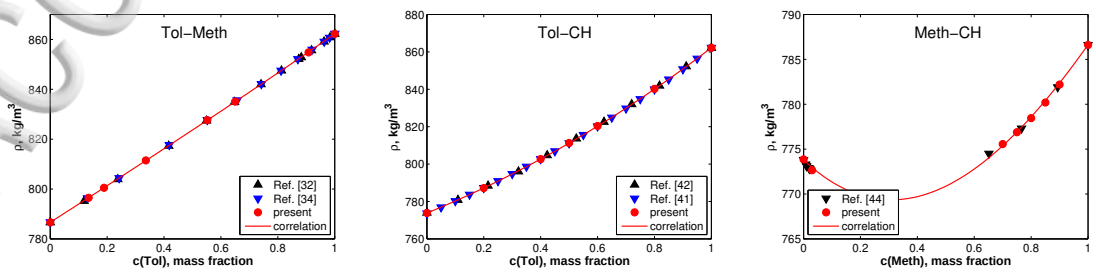

FIG. 7. Density of the mixtures.

Table IV, along with the coefficients of the polynomial model for the density, includes the absolute average deviation (AAD) between the experimental data and the model for both properties.

b. Thermal expansion coefficient

Similarly to density, the thermal expansion coefficient is presented by the coefficients of the power series polynomial as

$$\alpha(c) = -\frac{1}{\rho}\frac{\partial \rho}{\partial T} = a_0 + a_1 \cdot c + a_2 \cdot c^2 + a_3 \cdot c^3 \tag{16}$$

The coefficients a_i for the thermal expansion as well as the coefficients $\{A_0, A_1\}$ for the deviation are summarized in Table V. Figure 8 presents the fit results for the mixtures.

TABLE V. Polynomial coefficients for correlation of the thermal expansion coefficient for three considered binary mixtures at $T = 298.15\,\mathrm{K}$.

	Units	Tol–Meth	Tol–CH	Meth–CH
Deviation in thermal expansion coefficient, $\Delta\alpha$				
A_0	$10^{-3}\,\mathrm{K}^{-1}$	0.1101	0.0248	0.3031
A_1	$10^{-3}\,\mathrm{K}^{-1}$	−0.0541	0.0219	0.2712
Thermal expansion coefficient, α				
a_0	$10^{-3}\,\mathrm{K}^{-1}$	1.1990	1.2200	1.2200
a_1	$10^{-3}\,\mathrm{K}^{-1}$	−0.0610	−0.0913	0.5533
a_2	$10^{-3}\,\mathrm{K}^{-1}$	0.0523	−0.0906	−1.1166
a_3	$10^{-3}\,\mathrm{K}^{-1}$	−0.1082	0.0438	0.5423
AAD_α	%	0.17	0.15	0.28

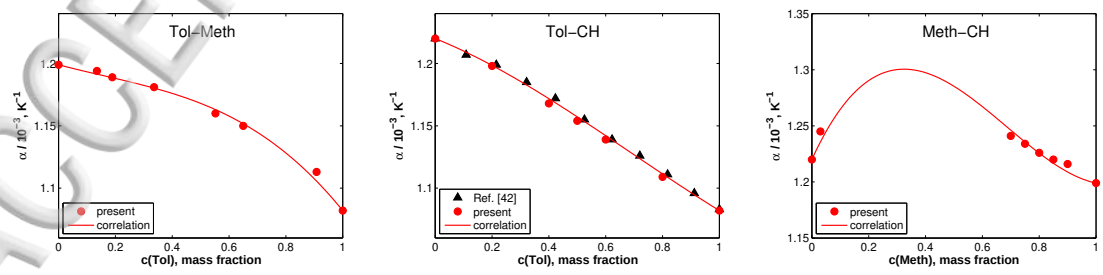

FIG. 8. Thermal expansion coefficients.

It follows from the table, that the concentration dependency $\alpha(c)$ is closest to the linear behaviour for the Tol–Ch mixture, as it has smallest $\{A_0, A_1\}$ coefficients. Despite its

smallness, the non-linearity can be clearly distinguished and fitted by the applied approach (as seen in Fig. 8(b)).

c. *Viscosity*

As all other properties, dynamic viscosity is also represented by a power series polynomial as

$$\mu(c) = \sum_{n=0}^{N} v_n c^n \,. \tag{17}$$

The polynomial coefficients for the obtained correlations are listed in Table VI and the fit result is shown in Fig. 9.

TABLE VI. Polynomial coefficients for correlation of dynamic viscosity for three considered binary mixtures at $T = 298.15\,\mathrm{K}$.

	Units	Tol–Meth	Tol–CH	Meth–CH
Deviation in viscosity, $\Delta\mu$				
A_0	mPa·s	0.0968	−0.4973	−0.4497
A_1	mPa·s	0.0051	−0.1880	−0.6628
A_2	mPa·s	−0.2037	–	−0.6039
A_3	mPa·s	0.2242	–	–
Dynamic viscosity, μ				
v_0	mPa·s	0.5470	0.8990	0.8990
v_1	mPa·s	0.1334	−1.0264	−2.0684
v_2	mPa·s	−0.6629	1.0615	5.4578
v_3	mPa·s	2.4158	−0.3761	−6.1571
v_4	mPa·s	−3.6687	–	2.4157
v_5	mPa·s	1.7934	–	–
AAD_μ	%	0.47	0.88	0.28

With this particular property we have got an exclusion from our common approach of fitting the property deviation by a two-term Redlich–Kister polynomial. To reconstruct a peculiarity of the concentration dependency of the viscosity for Tol–Meth mixture we had to apply up to four-term R-K polynomial. Similarly, for Meth–CH mixture a three-term R-K polynomial provided better correlation. The derived power series polynomials have been changed accordingly. Viscosity plots for the mixtures, presented in Fig. 9, confirm the need in more complex description and accuracy of the fit.

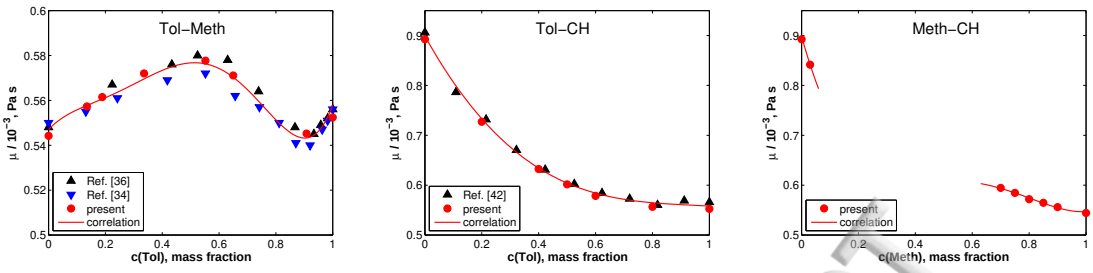

FIG. 9. Dynamic viscosity.

To conclude, this section presents most comprehensive and accurate correlations for basic physical properties of the considered binary mixtures. These correlations describe all mutually consistent datasets available in literature and measured in this work, and in the majority of cases deviate from reliable measurements by less than 1%.

B. Optical properties

The optical contrast factors, which have been measured as described in Section II D, are listed in Tables VII - IX. Measured refractive indices at 598.3 nm, which are necessary for concentration determination in the TGC technique[48] are also included for completeness. The experiments give a linear dependence in T (degree Celisus) for $(\partial n/\partial T)_{p,c}$. The resulting coefficients can then be fitted by a polynomial in the concentration, see Eq. (18). The concentration derivative $(\partial n/\partial c)_{p,c}$ at $T = 298.15\,\mathrm{K}$ can be determined from measured refractive indices $(T_0 = 293.15\,\mathrm{K})$ together with $(\partial n/\partial T)_{p,c}$ by Eq. (19), as outlined in[15]. Eqs. (18) and (19) give a parametrization of the contrast factors in concentration (weight fraction) and temperature (degree Celsius), valid for the wavelength 633 nm. The resulting coefficients a_{ij} are listed in Table X.

$$\left(\frac{\partial n}{\partial T}\right)_{p,c} = a_{10} + a_{11}\cdot c + a_{12}\cdot c^2 + (a_{20} + a_{21}\cdot c + a_{22}\cdot c^2)\cdot T \tag{18}$$

$$\left(\frac{\partial n}{\partial c}\right)_{p,T} = a_{01} + a_{02}\cdot 2c + (a_{11} + a_{12}\cdot 2c)(T - T_0) + \frac{1}{2}(a_{21} + a_{22}\cdot 2c)(T^2 - {T_0}^2) \tag{19}$$

Previous studies[15,29] have shown that mixing rules can provide good predictions for the optical contrast factors of regular solutions from density data for the mixture and the refractive indices of the pure compounds. In order to test the feasibility of this approach for the here investigated more complex systems with a polar compound and a miscibility gap, we have calculated the contrast factors based on the Looyenga model for the refractive index

TABLE VII. Optical properties of the Tol-Meth mixture.

c	n, 298.15 K	n, 293.15 K	$(\partial n/\partial T)/\ 10^{-4}$, K^{-1}	$(\partial n/\partial c)$
Tol	589.3 nm	632.6 nm	632.6 nm, 298.15 K	632.6 nm, 298.15 K
0	1.32638	1.32788	-4.0736	0.1494
0.135	1.34699			
0.189	1.35545	1.35660	-4.4071	0.1559
0.336	1.37889	1.37994	-4.6722	0.1610
0.552	1.41453	1.41577	-5.0346	0.1684
0.650	1.43128	1.43262	-5.2025	0.1718
0.908	1.47681	1.47952	-5.6081	0.1807
1	1.49379	1.49422	-5.6743	0.1838

TABLE VIII. Optical properties of the Tol-CH mixture.

c	n, 298.15 K	n, 293.15 K	$(\partial n/\partial T)/10^{-4}$, K^{-1}	$(\partial n/\partial c)$
Tol	589.3 nm,	632.6 nm	632.6 nm, 298.15 K	632.6 nm, 298.15 K
0	1.42338	1.42539	-5.5045	0.0505
0.20	1.43437	1.43673	-5.5266	0.0578
0.40	1.44868	1.44854	-5.5444	0.0651
0.50	1.45373	1.45515	-5.5512	0.0688
0.60	1.46094	1.46233	-5.5676	0.0724
0.80	1.47658	1.47754	-5.6099	0.0797
1	1.49379	1.49422	-5.6743	0.0870

of a K-component mixture (here $K = 2$)[15,29,49]:

$$n(c,T) = \left(\frac{1}{3\epsilon_0}\rho(c,T)N_A\sum_k^K \frac{c_k\alpha_k}{M_k} + 1\right)^{3/2} . \tag{20}$$

Here, ϵ_0 is the vacuum permittivity, N_A Avogadro's number, ρ the density of the mixture, M_k the molar weight and c_k the mass fraction of component k. The molecular polarizabilities α_k are obtained from Eq. (20) applied to the pure compounds. For the simple case of a temperature-independent molecular polarizability, the optical contrast factors are given by[15]:

$$\left(\frac{\partial n}{\partial T}\right)_{p,c} = \frac{3}{2}(n - n^{1/3})\frac{1}{\rho}\left(\frac{\partial \rho}{\partial T}\right)_{p,c} \tag{21}$$

TABLE IX. Optical properties of the Meth-CH mixture measured at $T = 298.15\,\mathrm{K}$. (*)this values has not been measured but obtained from the parameterization.

c, Meth	n, 298.15 K 589.3 nm	n, 293.15 K 632.6 nm	$(\partial n/\partial T)/10^{-4}$, K^{-1} 632.6 nm, 298.15 K	$(\partial n/\partial c)$ 632.6 nm, 298.15 K
0	1.42338	1.42539	-5.5045	-0.1207
0.03	1.41960	1.42210	-5.4646*	-0.1194
miscibility gap				
0.70	1.35193	1.35276	-4.5103	-0.0885
0.80	1.34296	1.34302	-4.4117	-0.0839
0.90	1.33445	1.33525	-4.2377	-0.0793
1	1.32638	1.32788	-4.0736	-0.0746

TABLE X. Experimentally determined matrix coefficients a_{ij} for the parametrization of the contrast factors $(\partial n/\partial T)_{p,c}$ and $(\partial n/\partial c)_{p,T}$ according to Eqs. (18) and (19), respectively.

	Units	Tol-Meth	Tol-Ch	Meth-Ch
a_{00}		1.3277	1.4253	1.4255
a_{01}	10^{-1}	1.5036	0.5054	-0.1214
a_{02}	10^{-2}	1.7096	1.8328	0.0230
a_{10}	$10^{-4}\ K^{-1}$	-4.0114	-5.3688	-5.3607
a_{11}	$10^{-4}\ K^{-1}$	-1.7065	-0.1580	1.2879
a_{12}	$10^{-6}\ K^{-1}$	5.0172	-9.2603	5.2481
a_{20}	$10^{-7}\ K^{-2}$	-2.2108	-5.6373	-5.7178
a_{21}	$10^{-7}\ K^{-2}$	-7.3737	5.6630	0.8857
a_{22}	$10^{-7}\ K^{-2}$	7.4218	-2.0504	2.3411

$$\left(\frac{\partial n}{\partial c}\right)_{p,T} = \frac{3}{2}(n - n^{1/3})\left(\frac{1}{\rho}\left(\frac{\partial \rho}{\partial c}\right)_{p,T} + \left[\frac{\alpha_1}{M_1} - \frac{\alpha_2}{M_2}\right]\left[\frac{\alpha_1}{M_1}c + \frac{\alpha_2}{M_2}(1-c)\right]^{-1}\right) \tag{22}$$

The results of these calculations are compared to the measured contrast factors in Fig. 10. Generally, the agreement is convincing. Both for $(\partial n/\partial T)_{p,c}$ and $(\partial n/\partial c)_{p,T}$ the deviations are of the order of one percent or below. Only for $(\partial n/\partial c)_{p,T}$ of Meth-CH there are noticeable discrepancies of up to eight percent, which might still be acceptable for an estimation of S_T and D_T in case of binary mixtures. Such an accuracy will, however, certainly not be sufficient for ternaries, where a precise knowledge of the contrast factor matrix is crucial for the transformation from the refractive index to the composition space. At the moment, we do not have good arguments as to why the Looyenga model shows a rather poor agreement

in case of the concentration derivative of the refractive index of Meth-CH, whereas the temperature derivatives of the same mixture are perfectly predicted. Additional work will be required to elucidate this particular weakness and, possibly, find a more appropriate description.

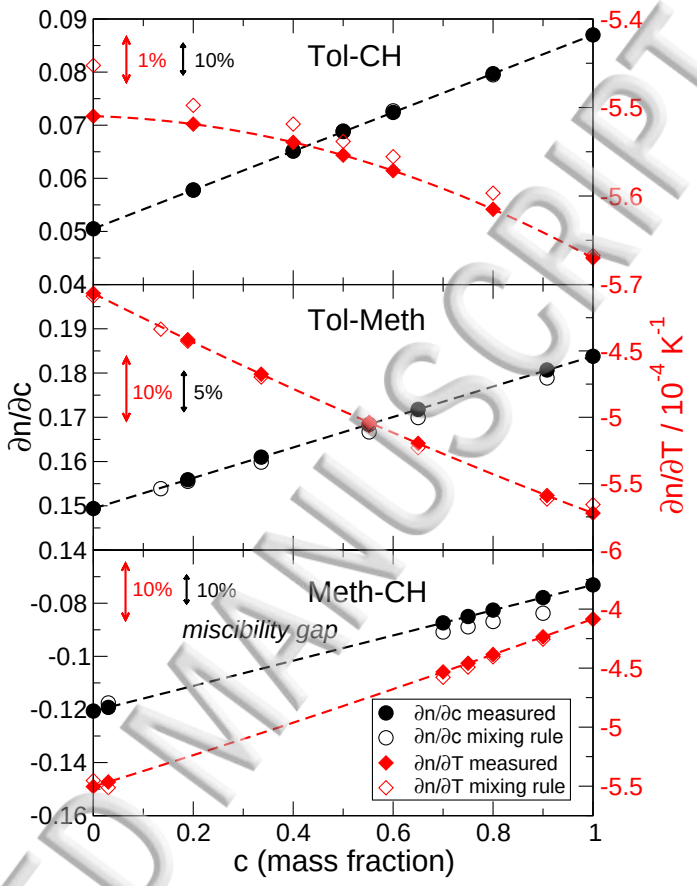

FIG. 10. Comparison of the measured contrast factors with predictions from the Looyenga mixing rule. The concentration always refers to the first component. Scale bars allow for an estimation of the relative errors.

C. Mass transport properties

The Fickian mass diffusion coefficients have been measured by two isothermal methods, sliding symmetric tubes (SST) at UM and counter flow cell (CFC) at ULB, and extracted from the thermodiffusion experiments using ODI and OBD. The Soret coefficients have been measured by means of the OBD and ODI techniques and thermodiffusion coefficients have been calculated as $D_T = S_T \cdot D$. The direct measurements of D_T were conducted in a thermogravitational column at UM. All results are summarized in Tables XI, XII, XIII and compared with available literature data.

TABLE XI. Diffusion, Thermal diffusion and Soret coefficients of Tol-Meth binary mixtures measured at $T = 298.15\,\mathrm{K}$.

c, Tol	$D/10^{-9}$ m^2 s^{-1}			$D_T/10^{-12}$ m^2 s^{-1} K^{-1}			$S_T/10^{-3}$ K^{-1}		
mass fr.	SST	OBD	ODI	TGC	OBD	ODI	(SST+TGC)	OBD	ODI
0.135	2.87			10.6			3.69		
0.189	2.49			8.6			3.45		
0.336	1.93	1.82		7.71	8.06		3.99	4.44	
0.500			1.14			5.50			4.82
0.552	1.17	1.023		5.03	4.14		4.32	4.05	
0.650	0.82	0.89	0.89	3.45	2.60	3.20	4.23	2.94	3.60
0.908		1.14			-8.20			-7.19	

TABLE XII. Diffusion, Thermal diffusion and Soret coefficients of Tol-Ch binary mixtures measured at $T = 298.15\,\mathrm{K}$. ISS[1] and ground[2] measurements in Ref.[14]. Spaces have been added

c, Tol	$D/10^{-9}$ m^2 s^{-1}		$D_T/10^{-12}$ m^2 s^{-1}K^{-1}	$S_T/10^{-3}$ K^{-1}
mass fr.	SST	OBD	OBD	OBD
0.150	1.77			
0.200		1.84	-6.20	-3.36
0.400	1.74	1.99	-4.99	-2.50
0.500		1.99	-4.39	-2.20
0.600	1.88	1.97	-3.47	-1.76
0.800		2.33	-2.36	-1.02
0.850	2.09			

Among the three binary pairs only Tol-Meth mixture has a large region with a positive Soret coefficient. Consequently, three principal techniques (TGC & SST, OBD and ODI) were used to determine the Soret, thermodiffusion and diffusion coefficients. Figure 11 summarizes all the results for this mixture and display excellent agreement between all measured Soret coefficients and literature data. A slight mismatch between the results of SST with Ref.[50] and Molecular Dynamic Simulations (MDS) from Ref.[51] for the diffusion coefficients at a low concentration of toluene leads to a small difference in the thermodiffusion coefficients. Actually, the authors of Ref.[50] did not measure diffusion coefficients and used available literature data.

The mixture Tol-Ch displays only negative Soret coefficients, and in the framework of this study the Soret coefficients were systematically measured using the OBD technique. For comparison, one of the points (c_{Tol}=0.4) was measured on the ISS. All the coefficients

TABLE XIII. Diffusion and Soret coefficients of Meth-Ch binary mixtures measured at $T = 298.15\,\mathrm{K}$. Spaces have been added

c,Meth	$D/10^{-9}\,\mathrm{m^2s^{-1}}$		$S_T/10^{-3}\,\mathrm{K^{-1}}$
mass fr.	SST	CFC	ULB
0.005		1.71	
0.010		1.23	
0.035		0.63	
0.650		0.37	
0.655		0.49	
0.665		0.64	
0.700		0.75	
0.750			-9.94
0.800	0.98		
0.885		1.75	
0.900	1.98		
0.990		2.32	

for this mixture are summarized in Fig. 12 along with previous results obtained by thermal diffusion forced Rayleigh scattering (TDFRS)[52,53] and Molecular Dynamic Simulations (MDS)[51]. All the measurements confirm that the Soret and thermodiffusion coefficients show almost linear concentration dependence. The mass diffusion coefficient does not show a pronounced concentration dependence and it reveals less favorable agreement between the data from different sources.

The most intriguing system is the Meth-Ch mixture, which has large demixing zone as shown in Fig. 1. The Soret coefficient from both sides of the demixing zone were previously measured[54] and revealed a negative sign of S_T at the right side demixing zone, in the region $c_{Meth} > 0.65$. On the left side, $c_{Meth} < 0.05$, the Soret coefficient is positive but still the mixture can be gravitationally unstable during the thermodiffusion experiment as the density shows anomalous behavior, $d\rho/dc < 0$, see Table I. Our measurements are focused on the diffusion coefficient on either side of the miscibility gap. The evolution of the diffusion coefficient with concentration shown in Fig. 14 exhibits sharp decrease of its value approaching phase boundaries. Let us analyze this behavior more carefully.

The present measurements were conducted at $T = 298.15\,\mathrm{K}$. The complete phase equilibrium curve (binodal) with a critical composition at $c_{cr} \approx 0.27$ and a critical temperature $T_{cr} \approx 320\,\mathrm{K}$ is shown in Fig. 13. We have included data from three different sources[55–57], which show noticeable scatter. Below the binodal is the spinodal. It touches the binodal in the critical point (top of curve), whose approximate locus[56,57] is indicated in Fig. 13.

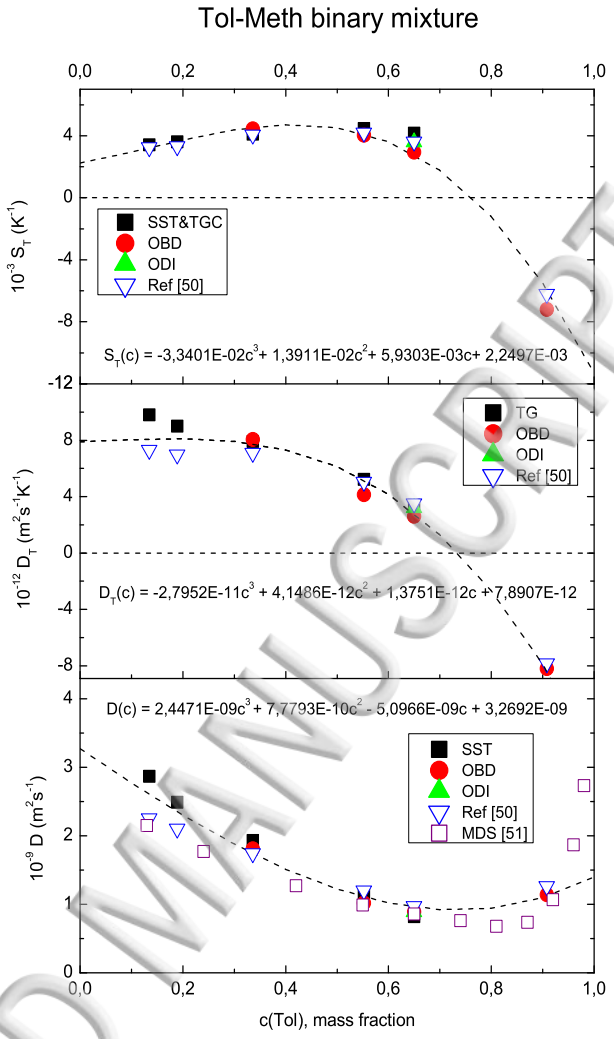

FIG. 11. Diffusive properties of Toluene-Methanol binary mixture as function of toluene mass fractions at $T = 298.15\,\mathrm{K}$. The fits were obtained from the experimental values of this work.

In the following we will attempt to obtain a simple scaling relation for the measured diffusion coefficient.

The diffusion coefficient of a critical mixture can be written as[58]

$$D = \frac{\alpha^b + \Delta\alpha}{S(0)} \ . \tag{23}$$

Here, α^b and $\Delta\alpha$ are the background contribution and the critical enhancement of the Onsager coefficient, respectively. $S(0)$ is the static structure factor[59]. Several Kelvin above the critical temperature T_c, the critical enhancement can be neglected and the structure factor shows classical mean field scaling $S(0) \sim \varepsilon^{-\gamma}$ with $\varepsilon = (T - T_c/T)$ and a scaling exponent of $\gamma = 1$. According to the pseudospinodal concept[60,61], a similar scaling is observed also

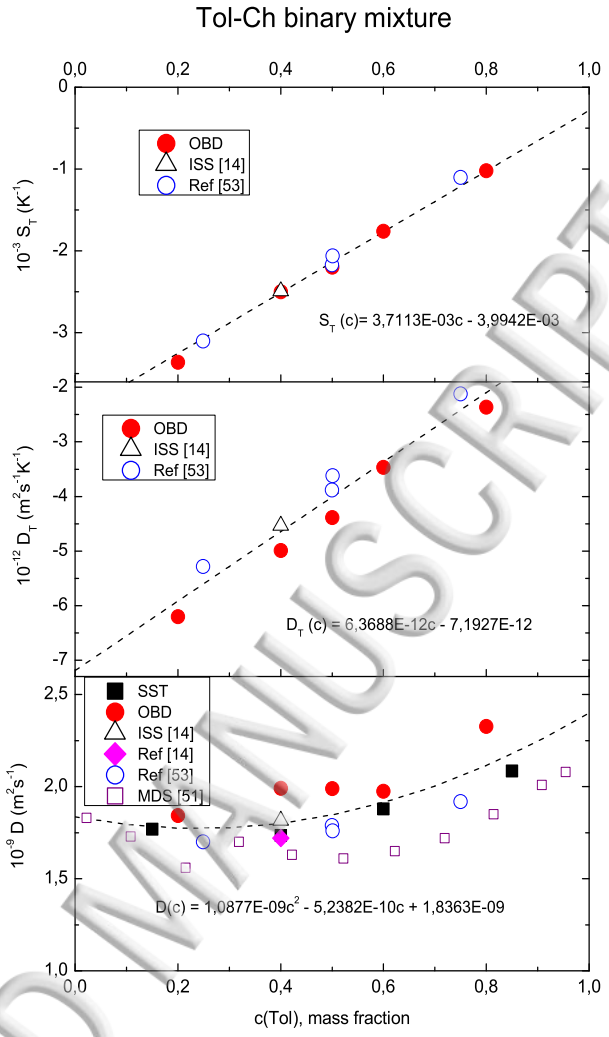

FIG. 12. Diffusive properties of Toluene-Cyclohexane binary mixture as function of toluene mass fractions at $T = 298.15\,\mathrm{K}$. The fits were obtained from the experimental values of this work.

for off-critical mixtures, provided the critical temperature T_c is replaced by the temperature T_{sp} of the spinodal. Assuming thermal activation with an activation temperature T_A for the Onsager coefficient α^b, the temperature dependence of the diffusion coefficient is eventually obtained as[62]

$$D = a_0 \frac{T - T_{sp}}{T} \exp(-T_A/T) \; . \tag{24}$$

Our experiments have not been performed at a fixed composition but at a constant temperature T, and the distance to the spinodal changes by variation of the composition c. With a few reasonable simplifications we can obtain an equivalent of Eq. (24) for the concentration variable. First, we assume a constant value for the Onsager coefficient α^b and, hence, for the proportionality constant a_0. Second, we approximate the spinodal to the

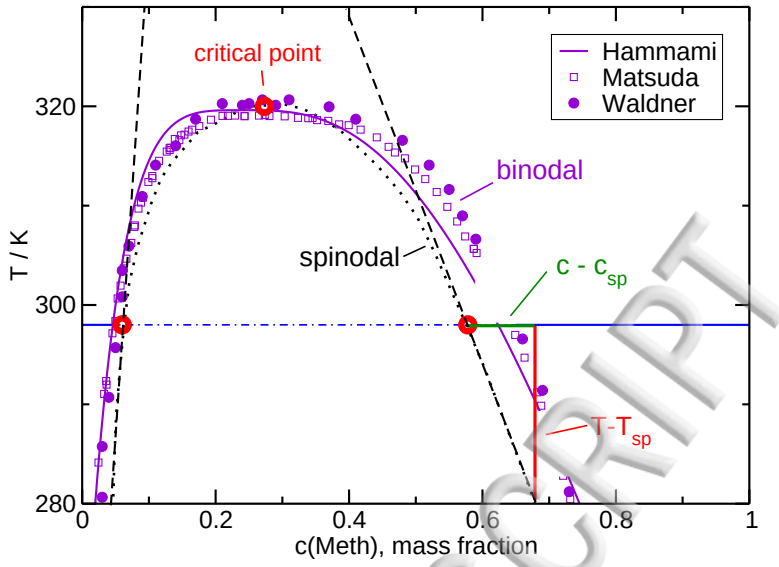

FIG. 13. The experimental data points indicate the binodal in Meth-Ch mixtures, which separates the homogeneous from the demixed state. Literature data from Hammami (Eq. (5) in the Ref.[57]), Matsuda[56] and Waldner[55] show a noticeable scatter. The dotted curve is a sketch to illustrate the spinodal. The horizontal blue lines outline the location of the current measurements. The dashed lines are approximate tangents to the spinodal at $T = 298.15\,\mathrm{K}$ (see text).

left and the right of the critical composition[55] $c_{cr} = 0.3$ by straight lines with slopes b_l and b_r, respectively (see Fig. 13). Hence, the distance to the spinodal along the temperature and the concentration axis below the critical point are related by $(T - T_{sp}) = b_x(c_{sp} - c)$, with b_x standing for b_l or b_r, respectively. Applying these assumptions to Eq. (24) results in an approximate scaling relation for the concentration dependence of the diffusion coefficient:

$$D = \frac{a_0}{T} \exp(-T_A/T)\; b_x(c_{sp} - c)\;. \tag{25}$$

Thus, the diffusion coefficient should decay roughly linear on approach of the spinodal. The extrapolation to the composition where D vanishes yields the approximate location of the spinodal at the experimental temperature $T = 298.15\,\mathrm{K}$.

As can be seen in Fig. 14, the decay of D is much steeper on the left side of the miscibility gap than on the right side. The intersections of the straight lines with the abscissa define the approximate locus of the spinodal. The steeper decay of D for low methanol concentrations is well described by a linear dependence according Eq. (25), i.e., $\gamma = 1$ and is in good agreement with the steeper slope of the binodal and, presumably, also the spinodal on this side.

We are well aware of the oversimplified treatment and the potentially questionable assumptions regarding the applicability of the scaling laws at a large distance from the spinodal. Neither the quality of the diffusion data nor the relatively crude approximations of our

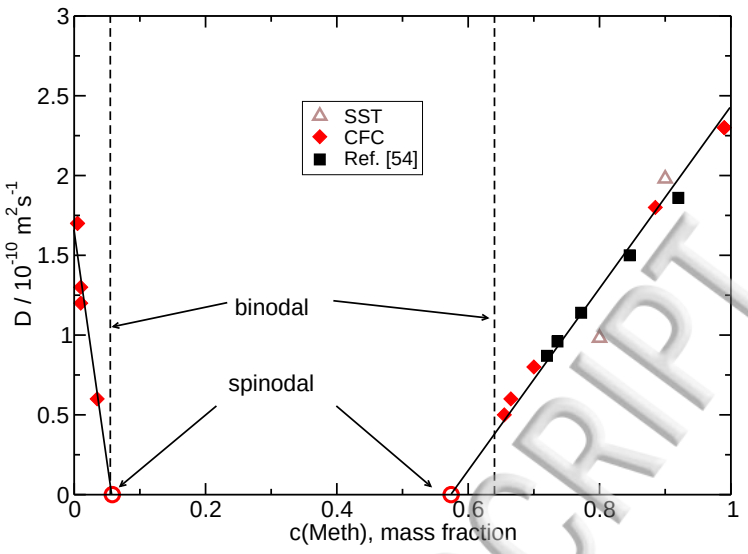

FIG. 14. Diffusion coefficient of the Methanol-Cyclohexane binary mixture at $T = 298.15\,\mathrm{K}$. The straight lines extrapolate to the spinodal.

model allow for a precise pinning down of the spinodal. Nevertheless, the general picture is in good agreement with our experimental results and correctly describes the essence of the underlying physics.

Notice that the scaling should not depend on the concentration units. Here the mass fraction was used, while transition to other units require the use of the molecular weight and density. The molecular weight and the density, which varies inconsiderably within the mean field region, will change the coefficient in Eq. (25) but not the scaling.

IV. CONCLUSIONS

We have analyzed physical, optical and transport properties of the three binary systems consisting of toluene, methanol, and cyclohexane by employing different experimental techniques that exist in the participating laboratories as well as measurements under microgravity conditions onboard the ISS. Five ternary mixtures of these compounds were recently under investigation in microgravity experiments in the DCMIX$_2$ project. Since experiments on ternary mixtures are much more complicated and error-prone than measurements on binaries, the goal of this work has been to frame the ternary parameter space by thoroughly investigating the boundaries along the binary composition lines. These data can later serve as reliable limiting cases to which the measurements of the binary systems can be extrapolated. The experimental results for the Soret (S_T), diffusion (D) and thermodiffusion (D_T) coefficients are in favorable agreement between different techniques and the existing literature values.

All binary pairs have regions with negative Soret coefficients, which may lead to a con-

native instability in the experiments with nonuniform temperature in a gravity field. The correlations for the thermophysical properties have been included in this study, because their knowledge is important for, e.g., the investigation of fingering buoyant instabilities in such systems.

In addition to the measured optical contrast factors $(\partial n/\partial c)_{p,T}$ and $(\partial n/\partial T)_{p,c}$, they were also calculated based on the Looyenga model. The overall agreement is excellent except for $(\partial n/\partial c)_{p,T}$ of Meth-CH, where discrepancies of up to eight percent have been noticed. Additional work will be required to find a more appropriate description. An approach similar to the Looyenga model would be very desirable in case of binary and – even more – ternary mixtures, since it would significantly ease the burden of a precise determination of the optical contrast factors by relating them to the usually more easily accessible thermal expansion coefficients in connection with the refractive indices of the pure compounds.

The careful measurements of the diffusion coefficient in the mixture Meth-Ch close to the miscibility gap have revealed a characteristic slowing down near the binodal. We have interpreted this in the spirit of the pseudospinodal concept, where scaling laws can also be observed for off-critical mixtures on approach of the spinodal, which is hidden under the binodal and not directly accessible. Using some plausible simplifications, we have postulated a mean field scaling exponent of $\gamma = 1$ for the diffusion coefficient D as a reasonable approximation not only along the temperature but also along the concentration axis.

V. ACKNOWLEDGEMENTS

This work has been supported by the PRODEX programme of the Belgian Federal Science Policy Office and ESA. The authors (ULB) are indebted to Prof. J.C. Legros (ULB, Brussels) for valuable discussions. The experiments at UB have been supported by Deutsche Forschungsgemeinschaft (Grant No. KO1541/9-2) and by Deutsches Zentrum für Luft- und Raumfahrt (Grant Nos. 50WM1130 and 50WM1544). Authors from UM would like to thank the support of MICRO4FAB, Research Groups (IT009-16)and Research Fellowship (Pre_2014_1_283) of Basque Government and TERDISOMEZ (FIS2014-58950-C2-1-P) of MINECO.

REFERENCES

[1] A. Mialdun, V. Shevtsova, J. Chem. Phys. **138**, 161102 (2013)
[2] M. Gebhardt, W. Köhler, J. Chem. Phys. **142**, 084506 (2015)
[3] A. Königer, H. Wunderlich, W. Köhler, J. Chem. Phys. **132**, 174506 (2010)
[4] A. Leahy-Dios, M.M. Bou-Ali, J.K. Platten, A. Firoozabadi, J. Chem. Phys. **122**, 234502.1 (2005)
[5] P. Blanco, M.M. Bou-Ali, J.K. Platten, D.A. De Mezquia, J.A. Madariaga, C. Santamaria, J. Chem. Phys. **132**, 114506 (2010)

[6]M. Bou-Ali, A. Ahadi, D. Alonso de Mezquia, Q. Galand, M. Gebhardt, O. Khlybov, W. Köhler, M. Larrañaga, J. Legros, T. Lyubimova et al., Eur. Phys. J. E **38** (2015)
[7]A. Mialdun, V. Sechenyh, J. Legros, J. Ortiz de Zárate, V. Shevtsova, J. Chem. Phys. **139**, 104903 (2013)
[8]J.C. Sechenyh, V.; Legros, V. Shevtsova, C.R. Mec. **341**, 490 (2013)
[9]M. Larrañaga, D. Rees, M. Bou-Ali, J. Chem. Phys. **140**, 054201 (2014)
[10]V. Shevtsova, Y.A. Gaponenko, V. Sechenyh, D.E. Melnikov, T. Lyubimova, A. Mialdun, J. Fluid Mech. **767**, 290 (2015)
[11]A. Mialdun, C. Minetti, Y. Gaponenko, V. Shevtsova, F. Dubois, Microgravity Sci. Tec. **25**, 83 (2013)
[12]A. Ahadi, S. Van Varenbergh, M.Z. Saghir, J. Chem. Phys. **138**, 204201 (2013)
[13]V. Shevtsova, V. Santos, C. Sechenyh, J.C. Legros, A. Mialdun, Microgravity Sci. Tec. **25**, 275 (2014)
[14]A. Mialdun, V. Shevtsova, J. Chem. Phys. **143**, 224902 (2015)
[15]M. Gebhardt, W. Köhler, A. Mialdun, V. Yasnou, V. Shevtsova, J. Chem. Phys. **138**, 114503 (2013)
[16]A. Mialdun, V. Yasnou, V. Shevtsova, A. Königer, W. Köhler, D. Alonso de Mezquia, M. Bou-Ali, J. Chem. Phys. **136**, 244512 (2012)
[17]A. Mialdun, V. Shevtsova, C.R. Mec. **339**, 362 (2011)
[18]A. Mialdun, V. Shevtsova, J. Chem. Phys. **134**, 044524 (2011)
[19]T. Kreis, *Handbook of Holographic Interferometry: Optical and digital Methods* (Wiley, 2005)
[20]A. Mialdun, J.C. Legros, V. Yasnou, V. Sechenyh, V. Shevtsova, Eur. Phys. J. E **38**, 27 (2015)
[21]M. Larrañaga, M. Mounir Bou-Ali, I. Lizarraga, J. Madariaga, C. Santamaria, J. Chem. Phys. **143**, 024202 (2015)
[22]M. Bou-Ali, O. Ecenarro, J. Madariaga, C. Santamaria, J. Valencia, J. Phys.: Condens. Matter **10**, 3321 (1998)
[23]J. Dutrieux, J. Platten, G. Chavepeyer, M. Bou-Ali, J. Phys. Chem. B **106**, 6104 (2002)
[24]R. Piazza, A. Guarino, Phys. Rev. Lett. **88**, 208302 (2002)
[25]A. Königer, B. Meier, W. Köhler, Philos. Mag. **89**, 907 (2009)
[26]A. Königer, H. Wunderlich, W. Köhler, J. Chem. Phys. **132**, 174506 (2010)
[27]P. Kolodner, H. Williams, C. Moe, J. Chem. Phys. **88**, 6512 (1988)
[28]G. Wittko, W. Köhler, Philos. Mag. **83**, 1973 (2003)
[29]W. Li, P. Segre, R. Gammon, J. Sengers, M. Lamvik, J. Chem. Phys. **101**, 5058 (1994)
[30]A. Becker, W. Köhler, B. Müller, Ber. Bunsenges. Phys. Chem. **99**, 600 (1995)
[31]R.K. Wanchoo, J. Narayan, Phys. Chem. Liq. **25**, 15 (1992)
[32]A. Rodríguez, J. Canosa, J. Tojo, J. Chem. Thermodyn. **33**, 1383 (2001)
[33]P. Rathore, M. Singh, Indian J. Chem. Sec. A **45A**, 2650 (2006)
[34]K.J. Han, J.H. Oh, S.J. Park, J. Chem. Eng. Data **51**, 1339 (2006)

[35]Z. Atik, J. Chem. Thermodyn. **38**, 201 (2006)
[36]P.S. Nikam, B.S. Jagdale, A.B. Sawant, M. Hasan, J. Chem. Eng. Data **45**, 559 (2000)
[37]A. Goyal, M. Singh, Indian J. Chem. Sec. A **46A**, 60 (2007)
[38]S.A. Sanni, C.J.D. Fell, H.P. Hutchison, J. Chem. Eng. Data **16**, 424 (1971)
[39]U.S. Pandey, S.N. Pandey, M. Kiranmayee, Asian J. Chem. **8**, 378 (1996)
[40]H. Iloukhani, M. Rezaei-Sameti, H. Zarei, Thermochim. Acta **438**, 9 (2005)
[41]T. Merzliak, I. Bartusseck, S. Stapf, M.A. Voda, B. Blümich, A. Pfennig, Fluid Phase Equilib. **245**, 158 (2006)
[42]A.A. Silva, R.A. Reis, M.L.L. Paredes, J. Chem. Eng. Data **54**, 2067 (2009)
[43]J.D. Pandey, A.K. Shukla, V. Sanguri, S. Pandey, J. Solution Chem. **24**, 1191 (1995)
[44]J. Canosa, A. Rodríguez, J. Tojo, J. Chem. Eng. Data **46**, 846 (2001)
[45]C. Houessou, P. Guenoun, R. Gastaud, F. Perrot, D. Beysens, Phys. Rev. A **32**, 1818 (1985)
[46]E.W. Lemmon, M.L. Huber, M.O. McLinden, *Nist standard reference database 23: Reference fluid thermodynamic and transport properties-refprop, version 9.1* (2013), `https://www.nist.gov/srd/refprop`
[47]O. Redlich, A.T. Kister, Ind. Eng. Chem. **40**, 345 (1948)
[48]M. Larrañaga, M.M. Bou-Ali, D.A. de Mezquia, D.A.S. Rees, J.A. Madariaga, C. Santamaria, J.K. Platten, Eur. Phys. J. E **38**, 28 (2015)
[49]H. Looyenga, Mol. Phys. **9**, 501 (1965)
[50]M. Bou-Ali, O. Ecenarro, J. Madariaga, C. Santamaria, J. Valencia, Phys. Rev. E **62**, 1420 (2000)
[51]G. Guevara-Carrion, T. Janzen, Y.M. Muñoz-Muñoz, J. Vrabec, J. Chem. Phys. **144**, 124501 (2016)
[52]G. Wittko, W. Köhler, J. Chem. Phys. **123**, 14506 (2005)
[53]G. Wittko, Ph.D. thesis, Universität Bayreuth (2007)
[54]M.J. Story, J.C.R. Turner, Trans. Faraday Soc. **65**, 2906 (1969)
[55]P. Waldner, H. Gamsjager, J. Solution Chem. **29**, 505 (2000)
[56]H. Matsuda, K. Ochi, K. Kojima, J. Chem. Eng. Data **48**, 184 (2003)
[57]N.E. Hammami, M. Bouanz, A. Toumi, Fluid Phase Equil. **384**, 25 (2014)
[58]J. Luettmer-Strathmann, *Thermal Nonequilibrium Phenomena in Fluid Mixtures* (Springer, 2002)
[59]M. Theobald, G. Meier, Phys. Rev. E **51**, 5776 (1995)
[60]B. Chu, F.J. Schoenes, M.E. Fisher, Phys. Rev. **185**, 219 (1969)
[61]S. Eckert, S. Hoffmann, G. Meier, I. Alig, Phys. Chem. Chem. Phys. **4**, 2594 (2002)
[62]A. Voit, A. Krekhov, W. Köhler, Phys. Rev. E **76**, 011808 (2007)

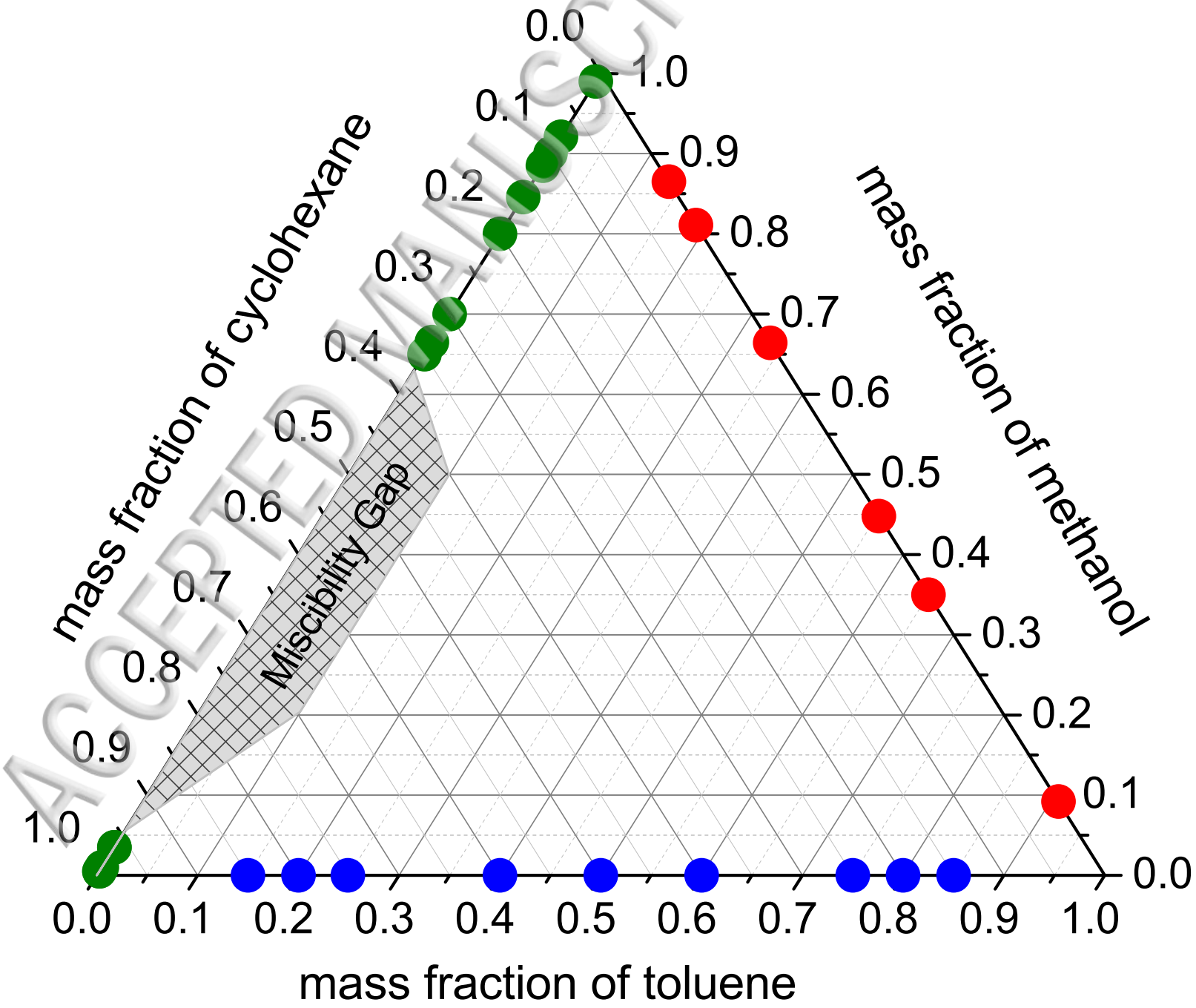

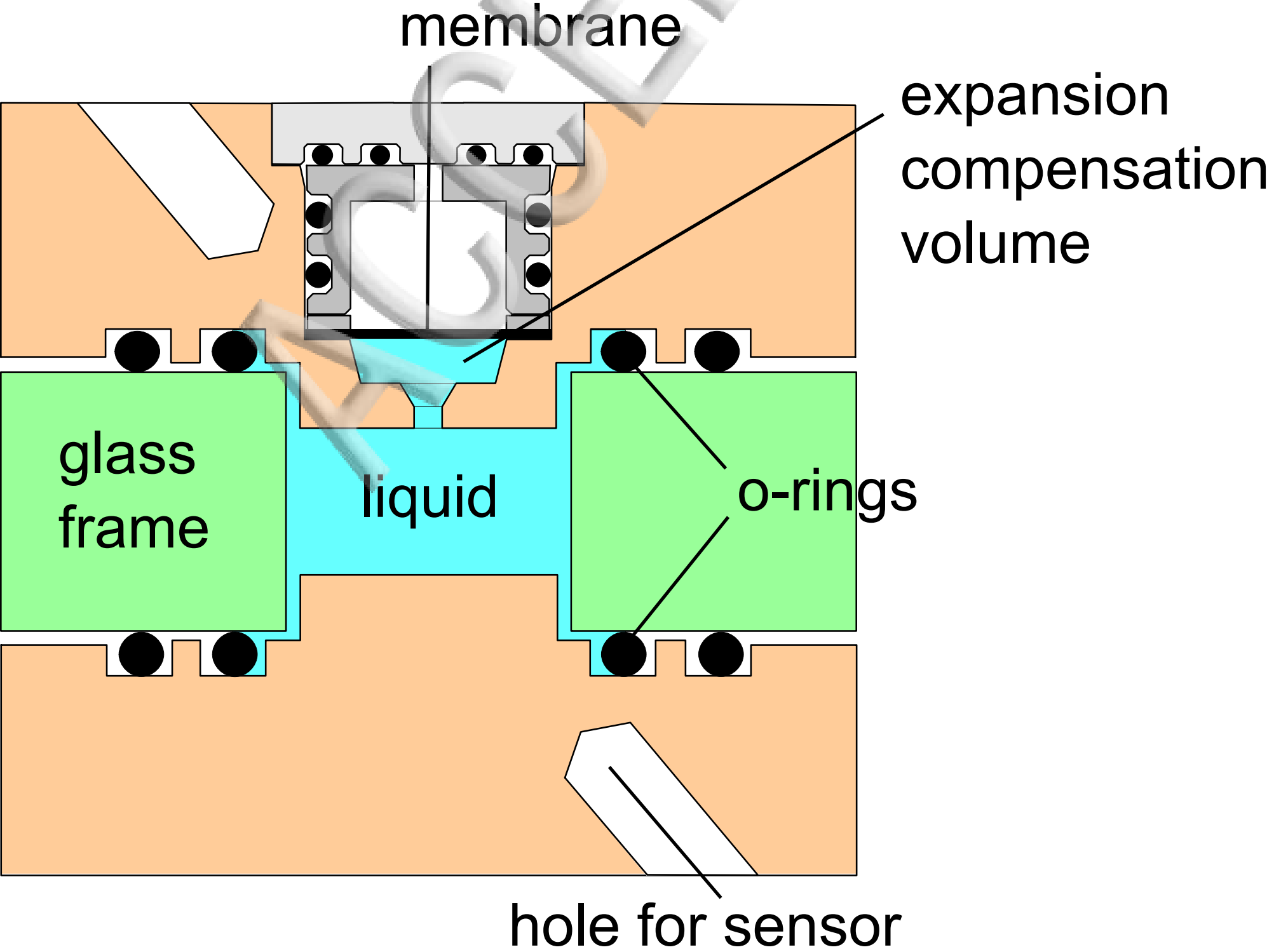
membrane
expansion
compensation
volume
glass
frame
liquid
o-rings
hole for sensor

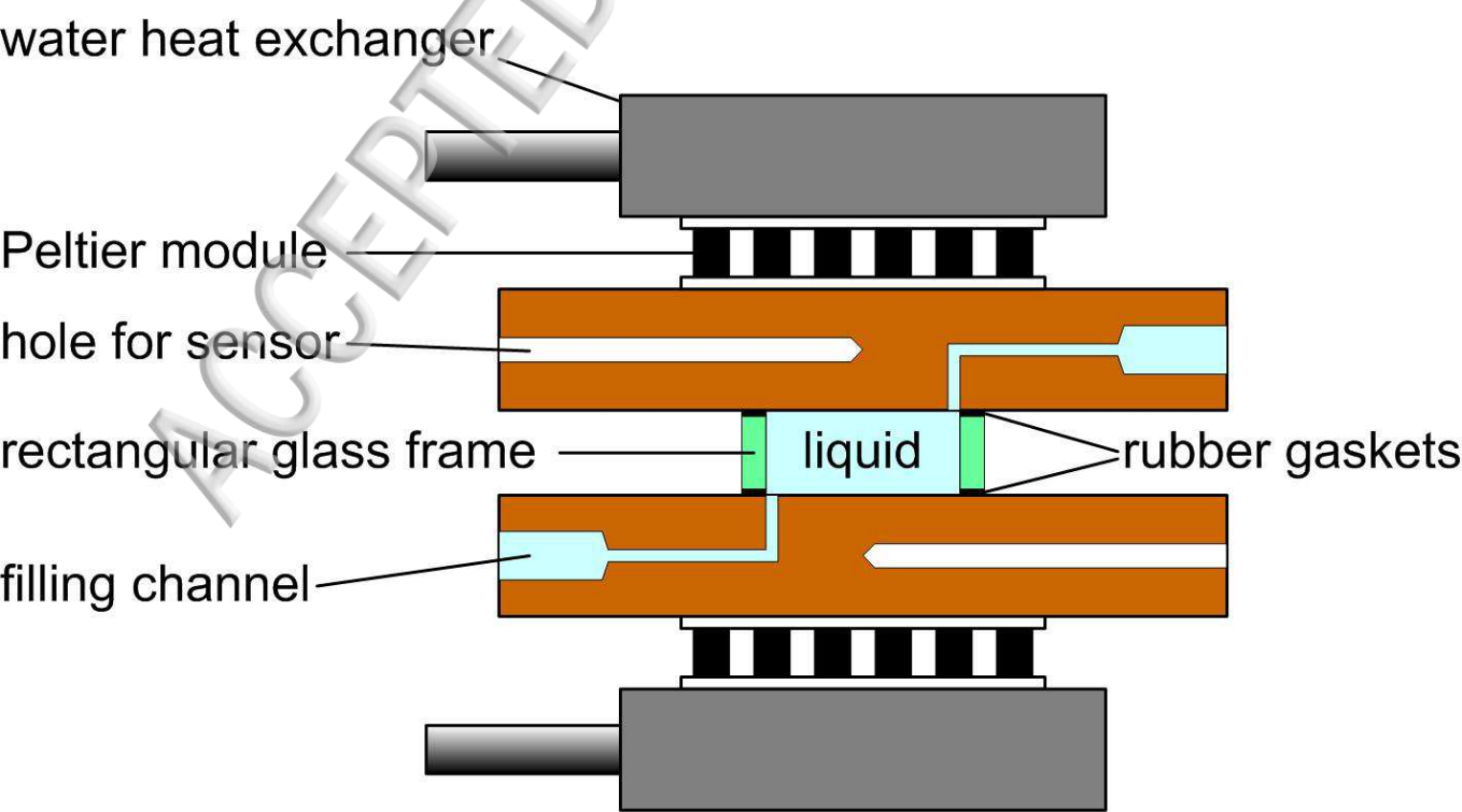
water heat exchanger
Peltier module
hole for sensor
rectangular glass frame
liquid
rubber gaskets
filling channel

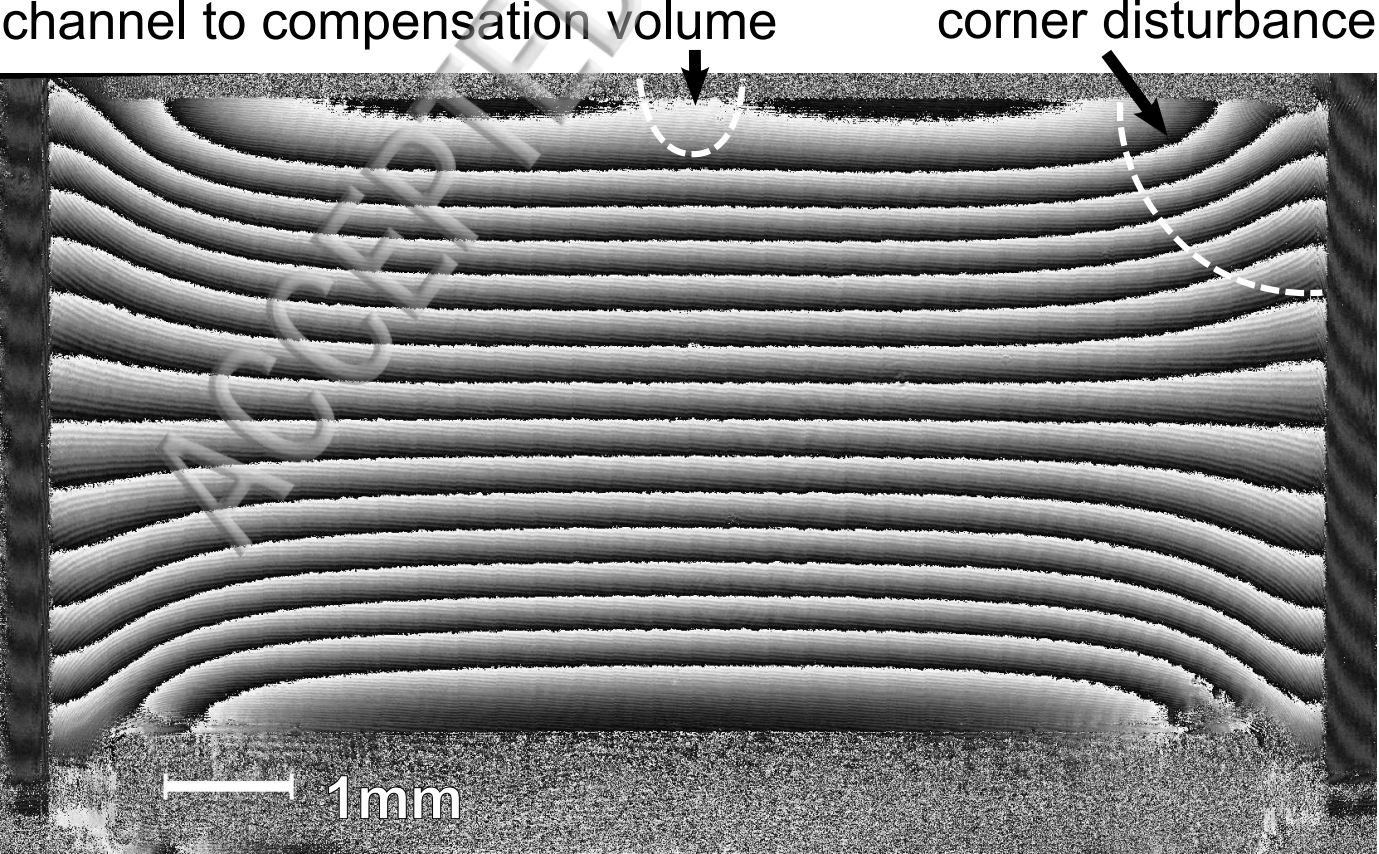
channel to compensation volume
corner disturbance
1mm

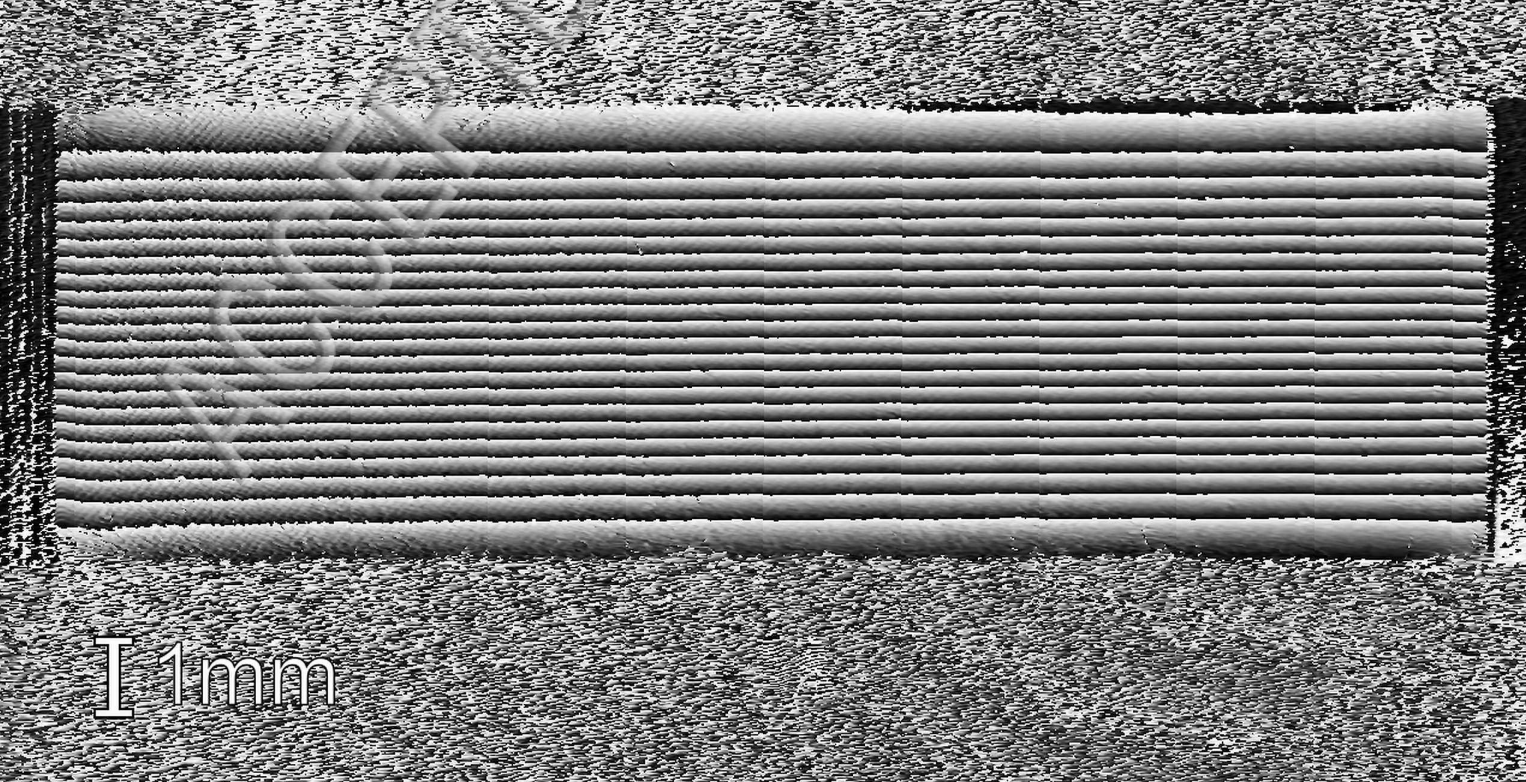
1mm

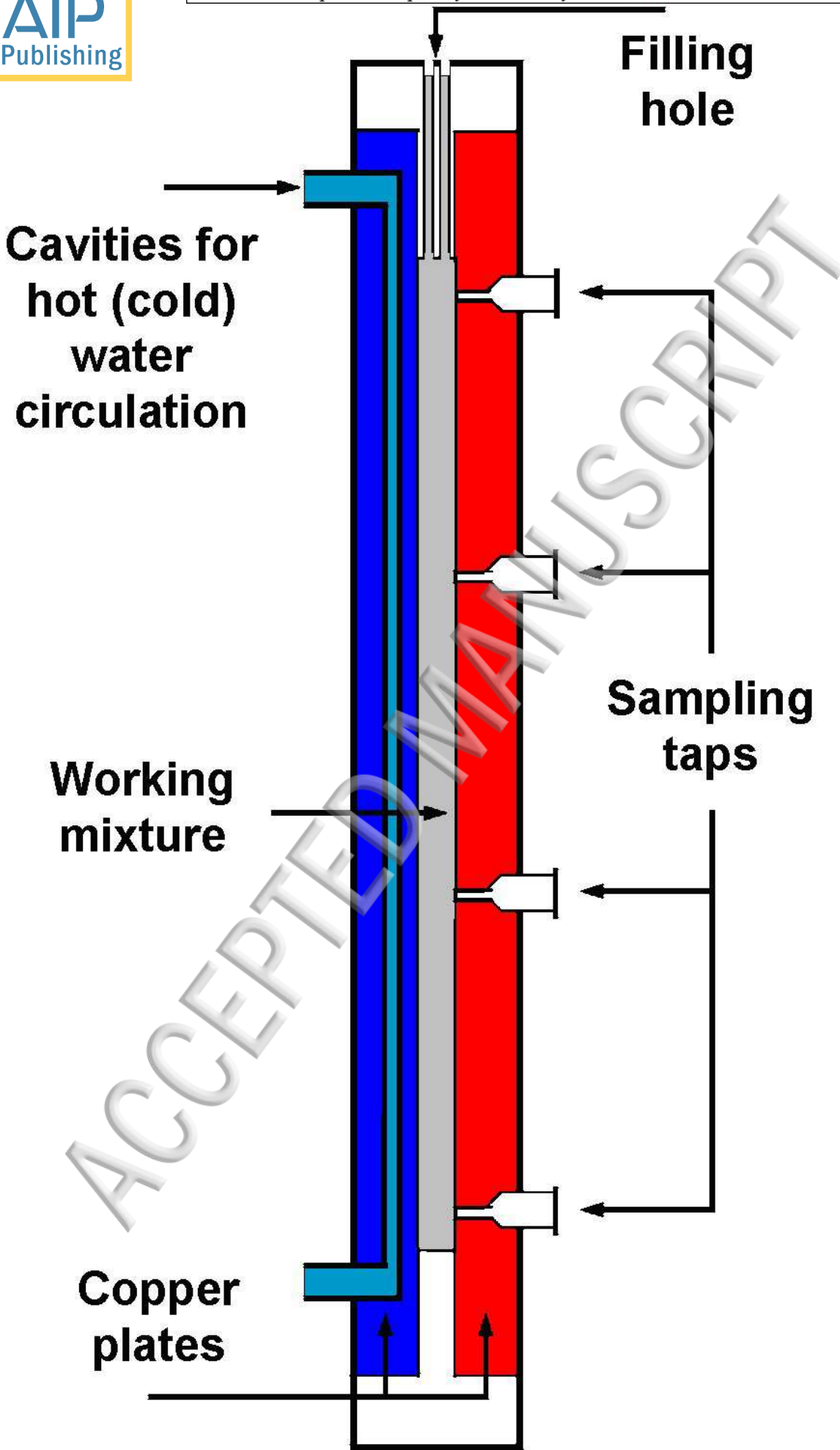

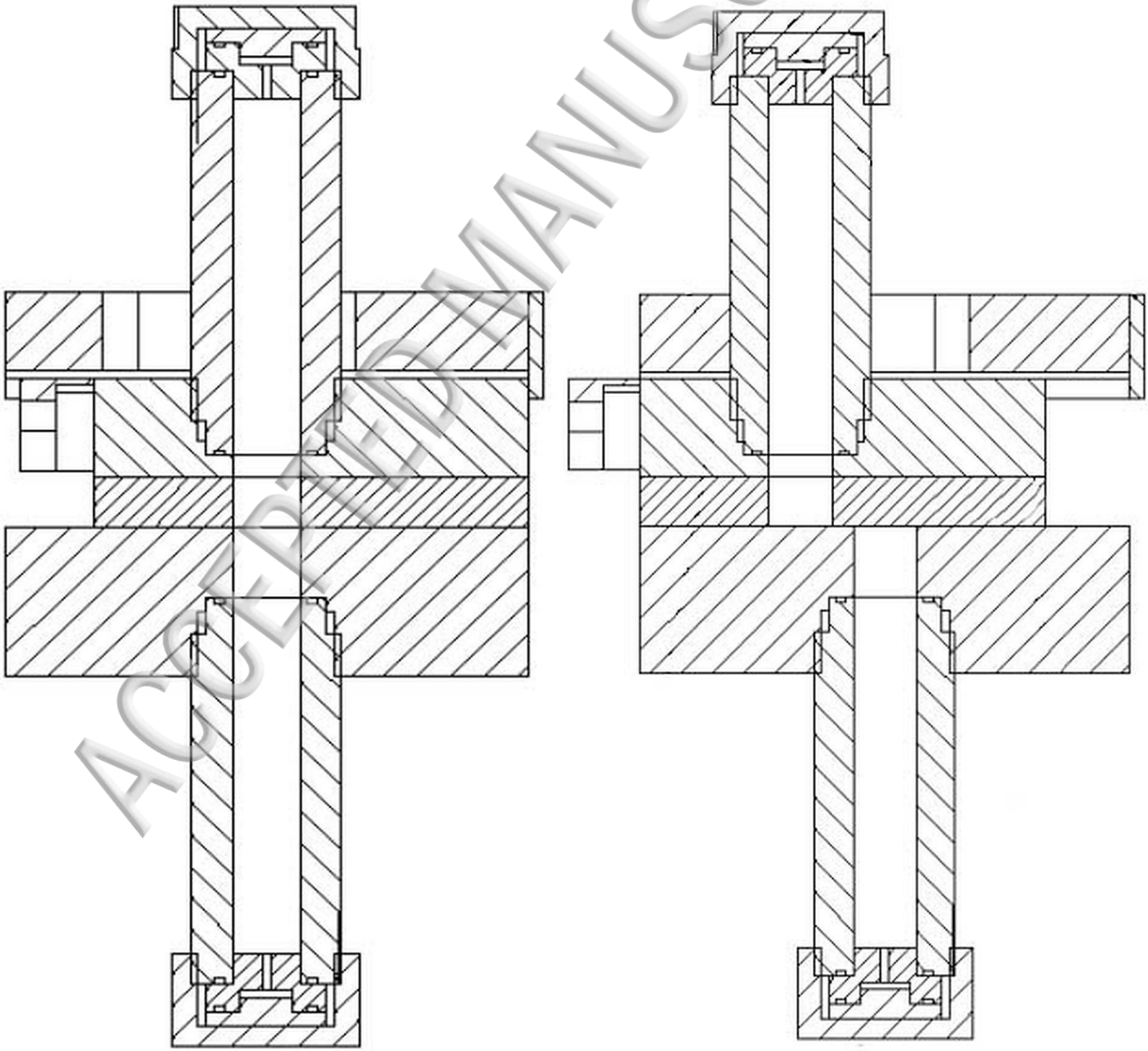

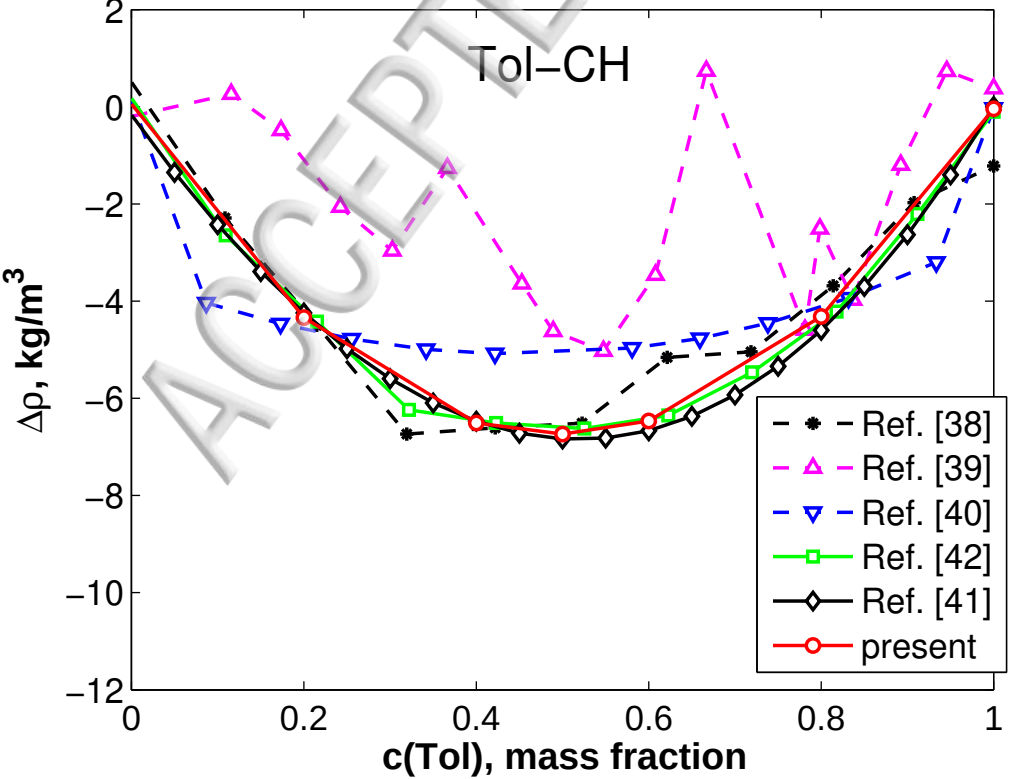
Tol–CH
Δρ, kg/m3
c(Tol), mass fraction
2
0
−2
−4
−6
−8
−10
−12
0
0.2
0.4
0.6
0.8
1
Ref. [38]
Ref. [39]
Ref. [40]
Ref. [42]
Ref. [41]
present

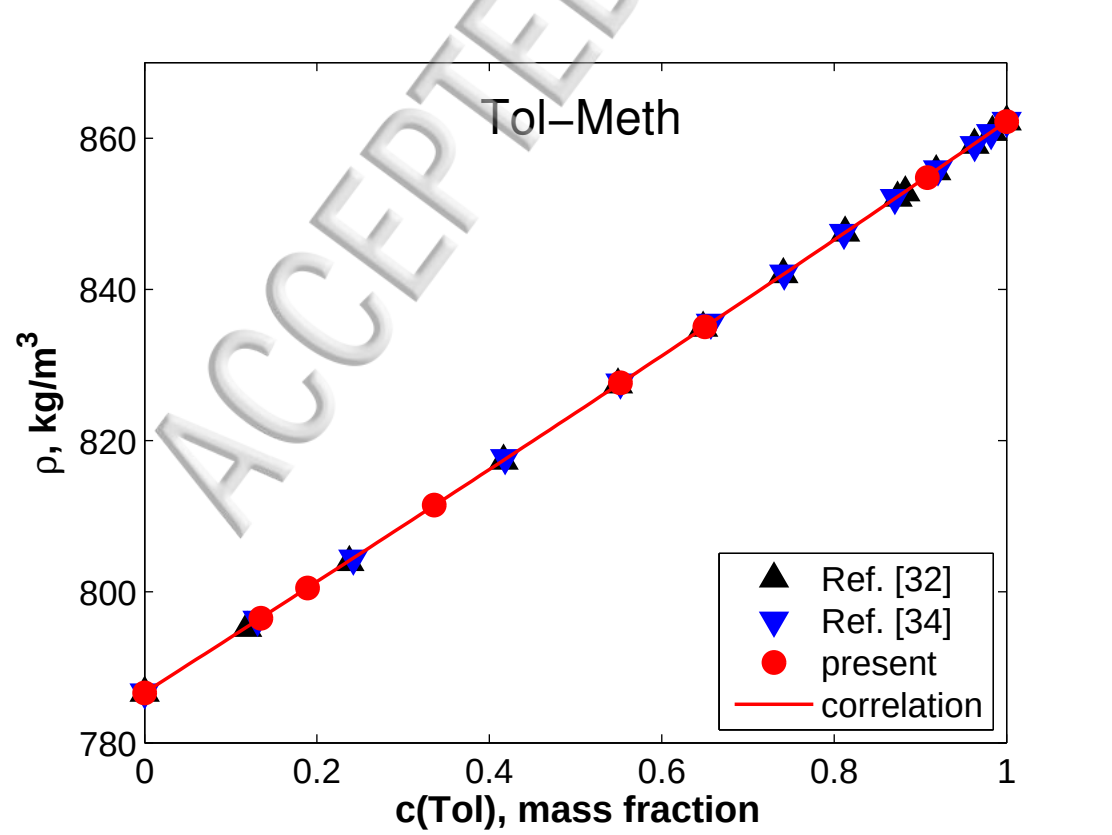
Tol–Meth
ρ, kg/m3
c(Tol), mass fraction
780
800
820
840
860
0
0.2
0.4
0.6
0.8
1
Ref. [32]
Ref. [34]
present
correlation

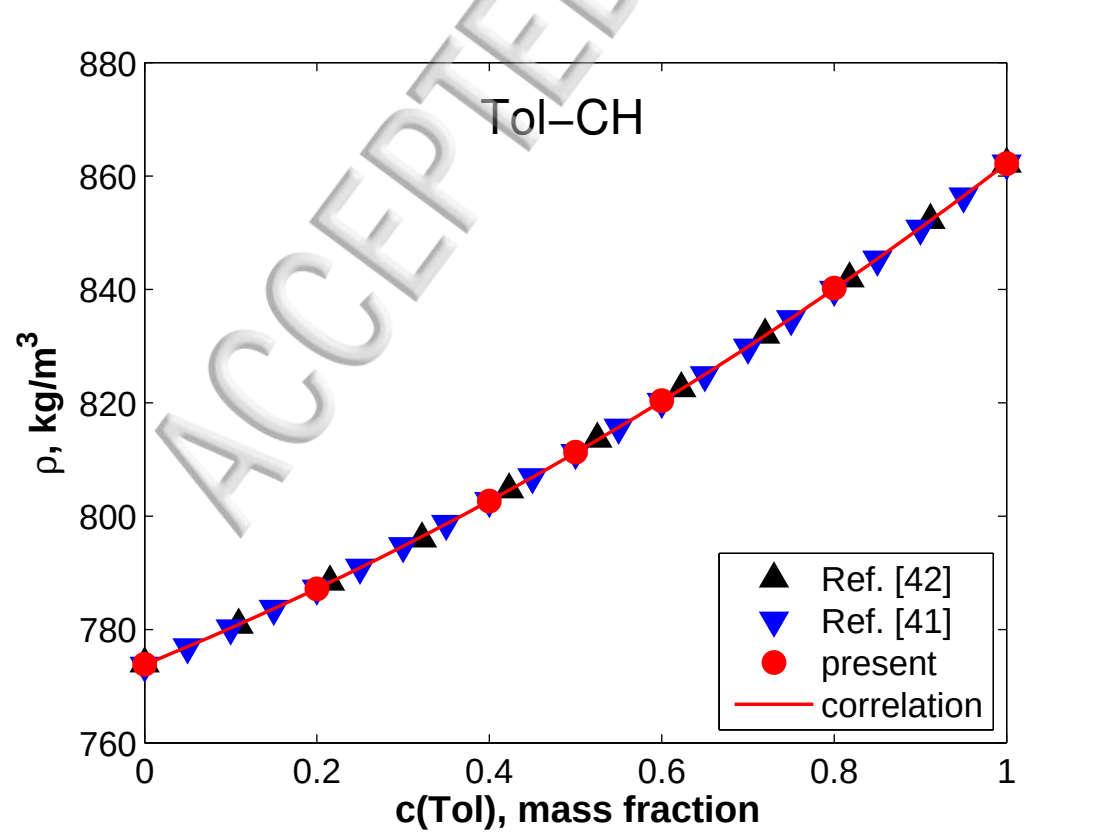
Tol–CH
ρ, kg/m3
c(Tol), mass fraction
880
860
840
820
800
780
760
0
0.2
0.4
0.6
0.8
1
Ref. [42]
Ref. [41]
present
correlation

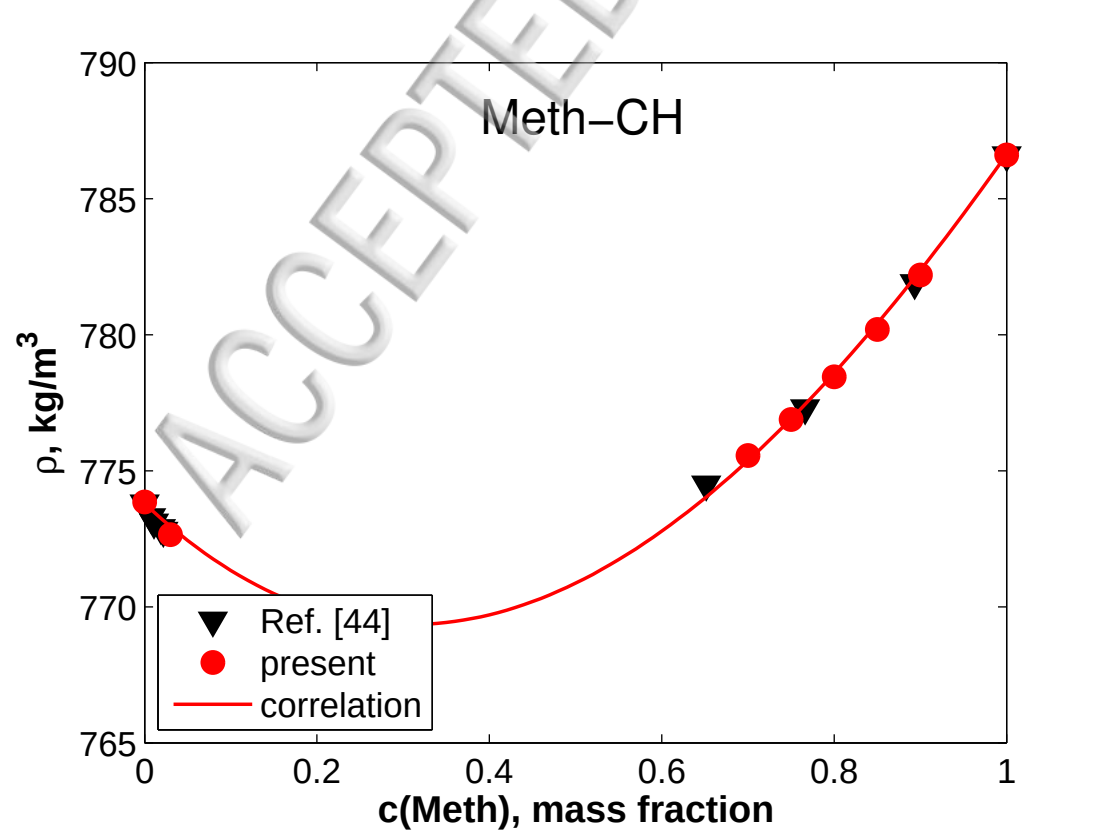
Meth–CH
ρ, kg/m3
c(Meth), mass fraction
790
785
780
775
770
765
0
0.2
0.4
0.6
0.8
1
Ref. [44]
present
correlation

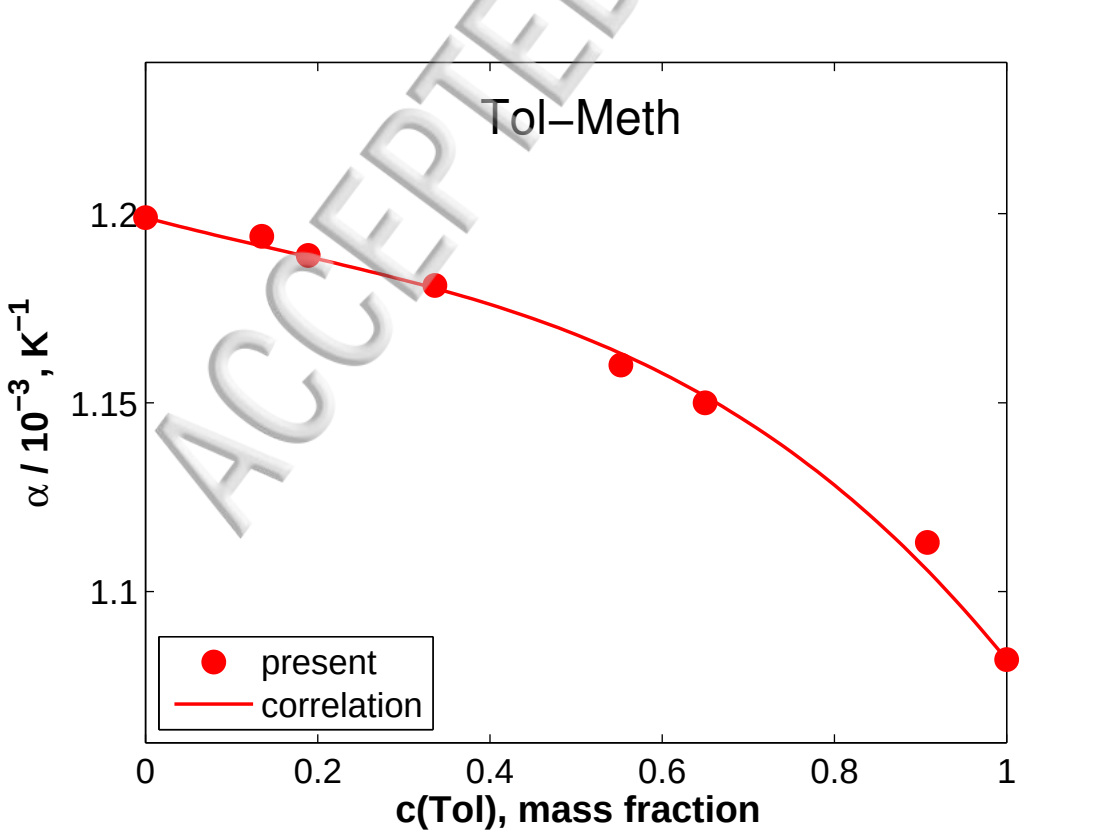
Tol–Meth
1.2
1.15
1.1
α / 10^−3, K^−1
present
correlation
0
0.2
0.4
0.6
0.8
1
c(Tol), mass fraction

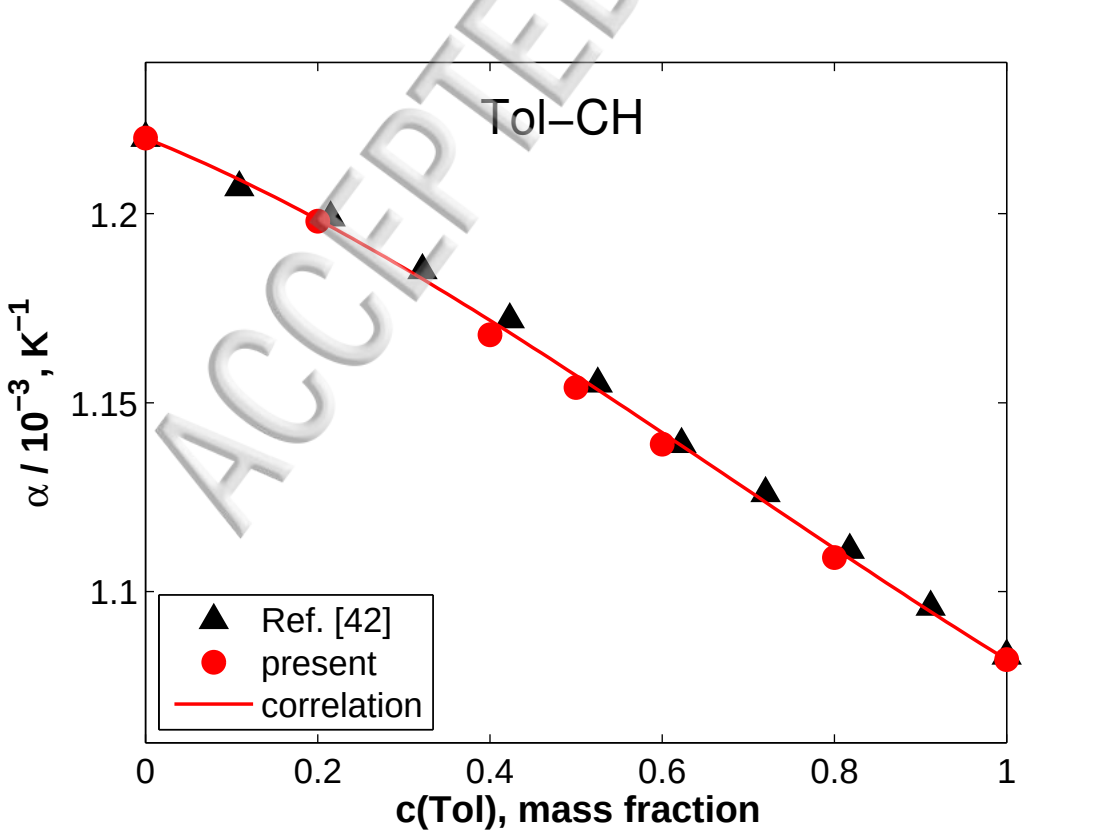
Tol–CH
1.2
1.15
1.1
α / 10^−3, K^−1
Ref. [42]
present
correlation
0
0.2
0.4
0.6
0.8
1
c(Tol), mass fraction

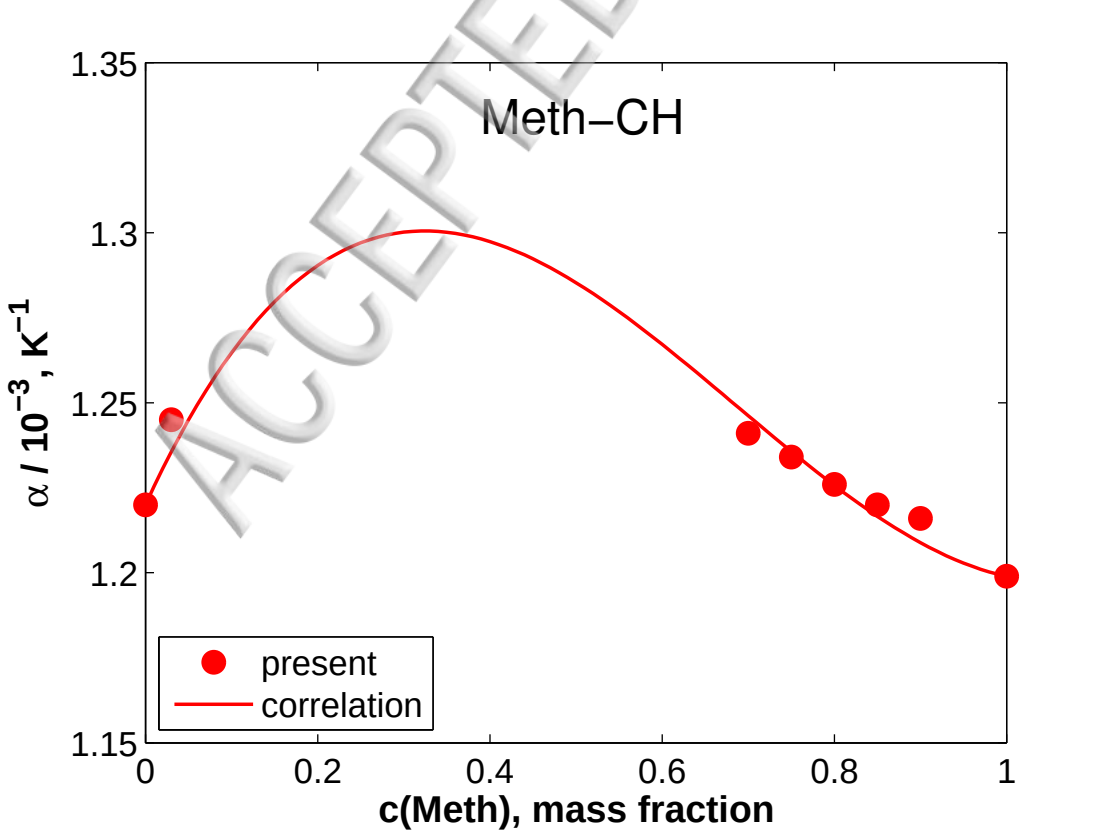
Meth–CH
α / 10^−3, K^−1
1.35
1.3
1.25
1.2
1.15
0
0.2
0.4
0.6
0.8
1
c(Meth), mass fraction
present
correlation

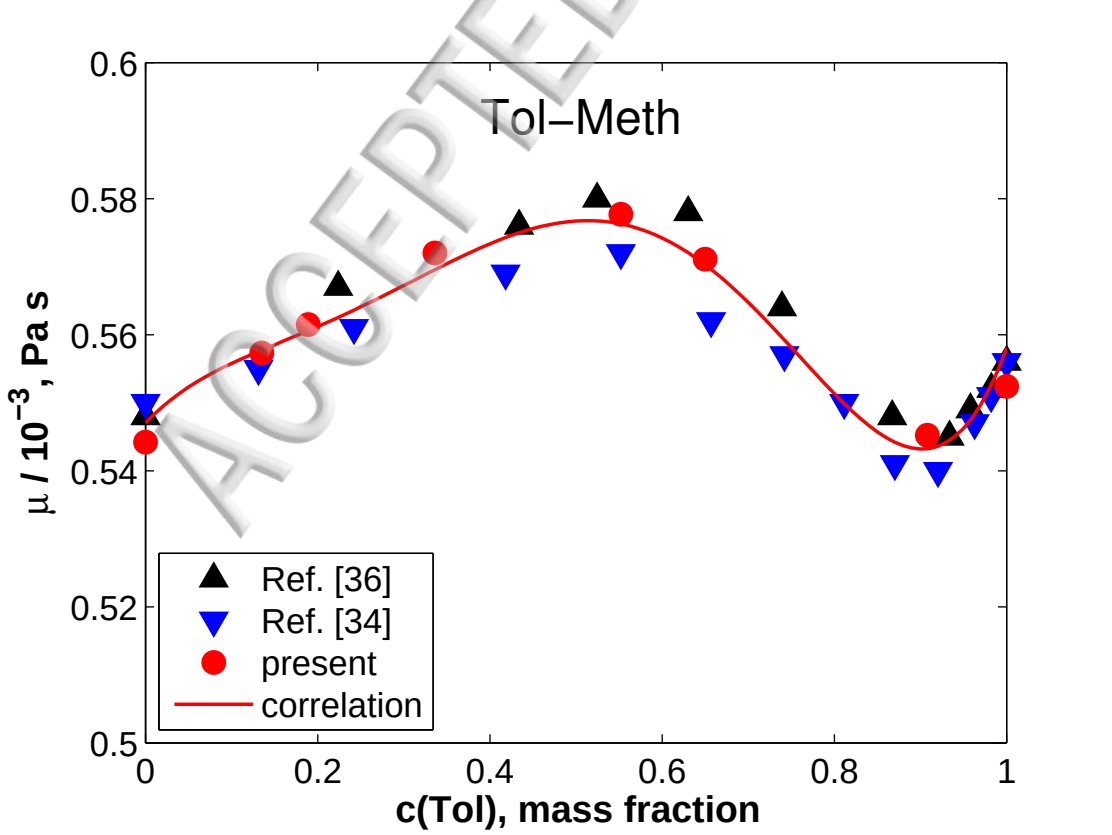
Tol–Meth
μ / 10⁻³, Pa s
c(Tol), mass fraction
0.6
0.58
0.56
0.54
0.52
0.5
0
0.2
0.4
0.6
0.8
1
Ref. [36]
Ref. [34]
present
correlation

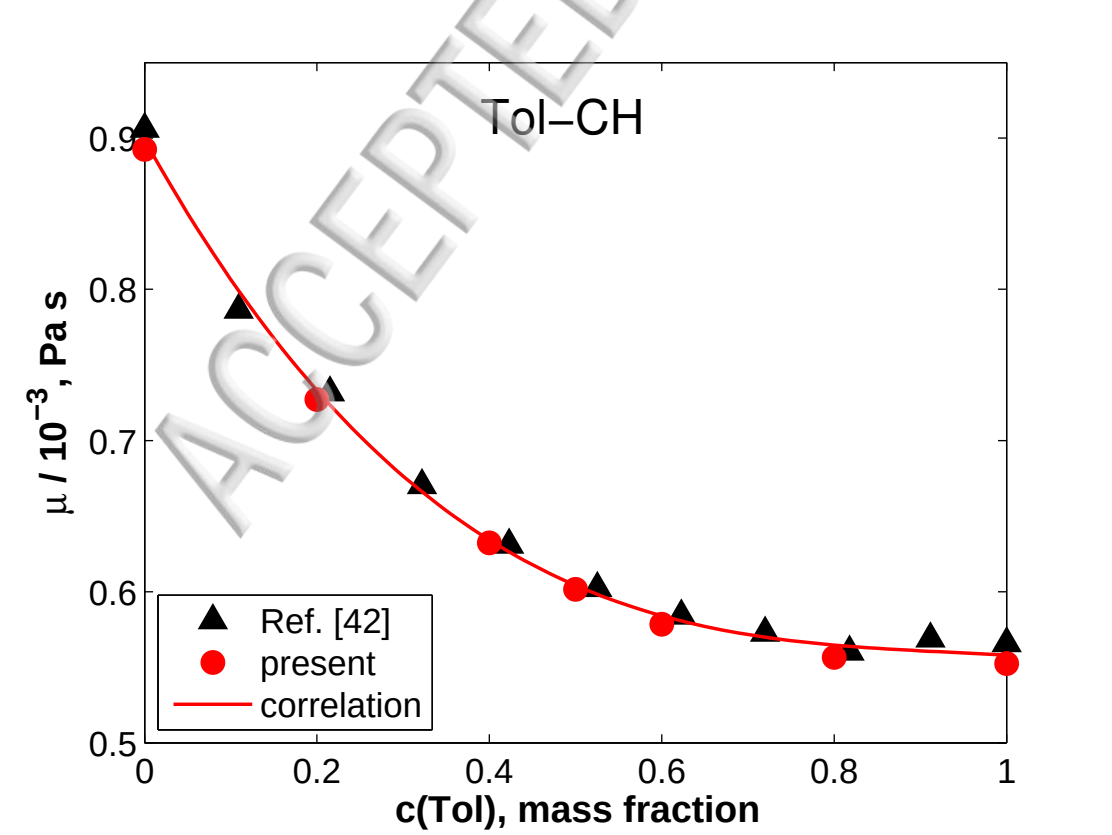
Tol–CH
μ / 10−3, Pa s
0.9
0.8
0.7
0.6
0.5
0
0.2
0.4
0.6
0.8
1
c(Tol), mass fraction
Ref. [42]
present
correlation

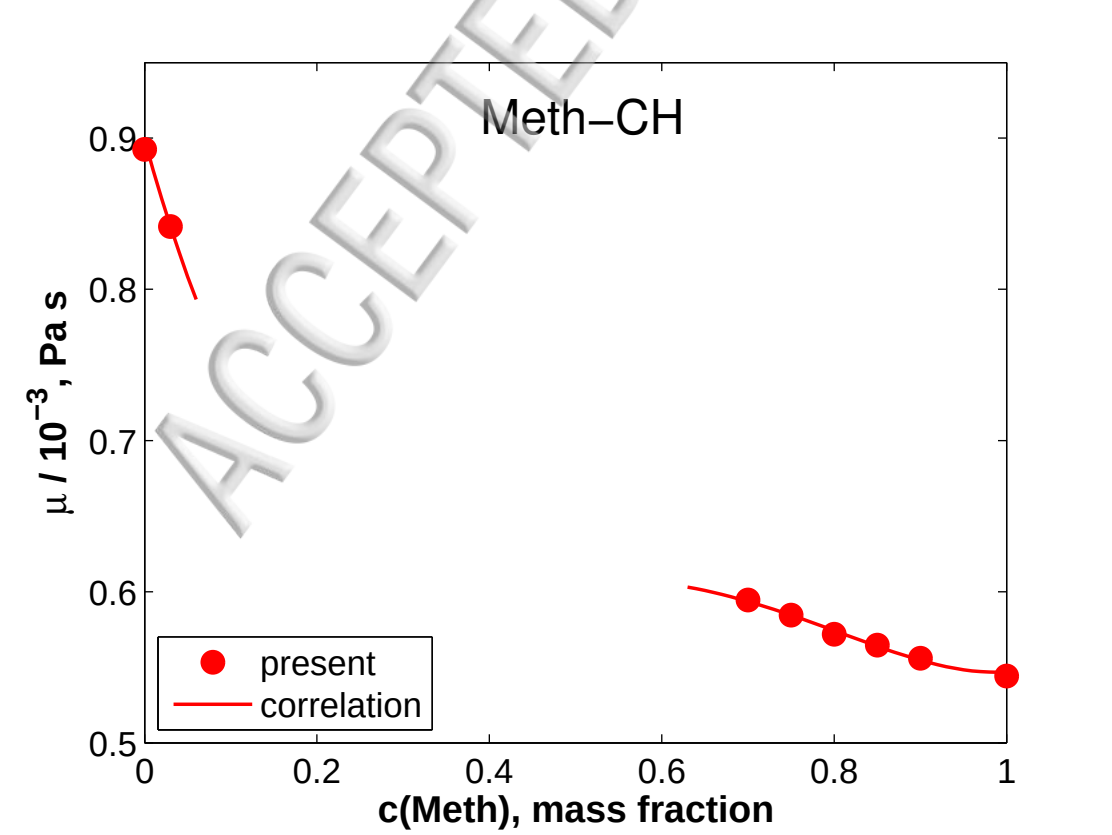
Meth–CH
μ / 10^−3, Pa s
0.9
0.8
0.7
0.6
0.5
0
0.2
0.4
0.6
0.8
1
c(Meth), mass fraction
present
correlation

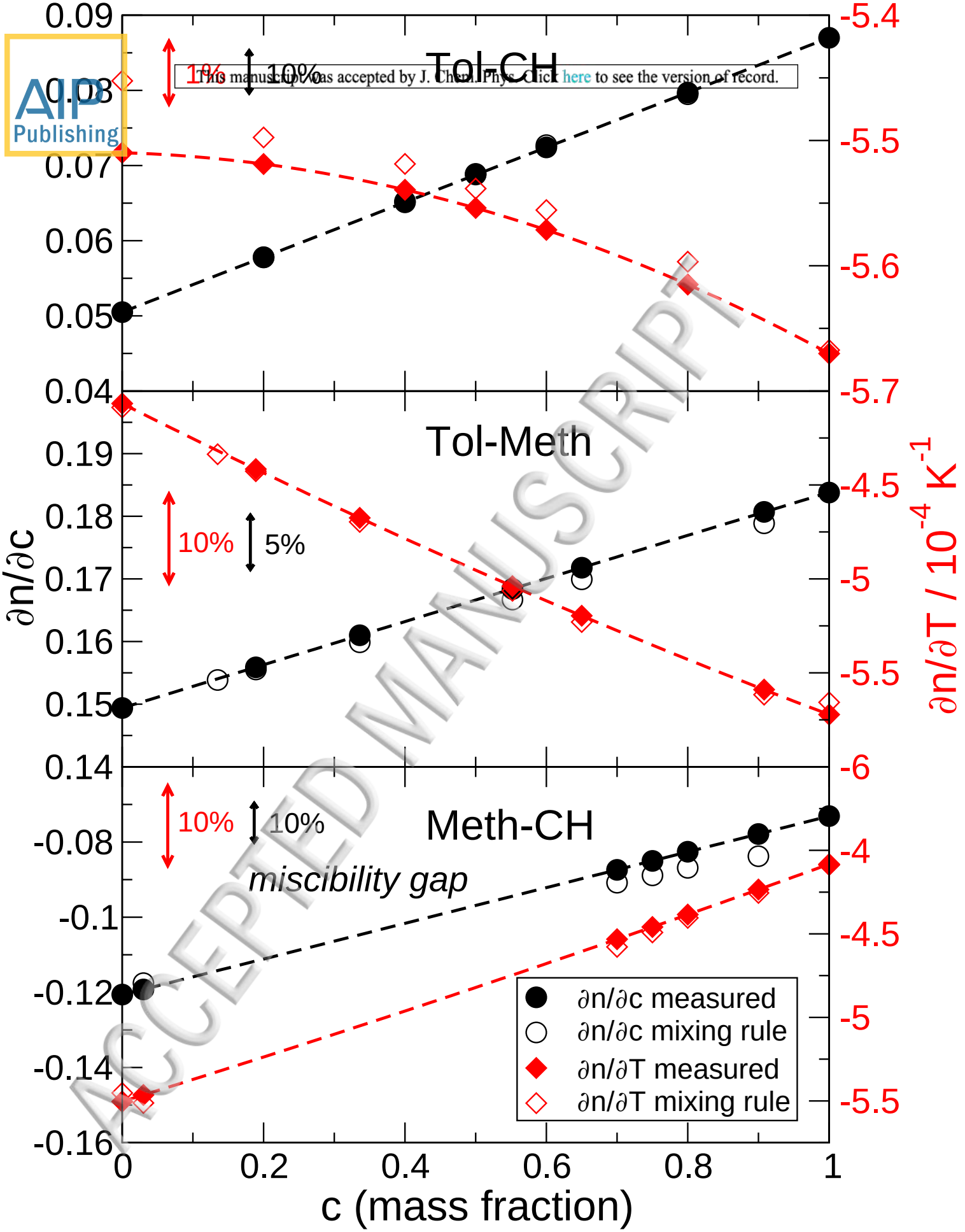

Tol-Meth binary mixture

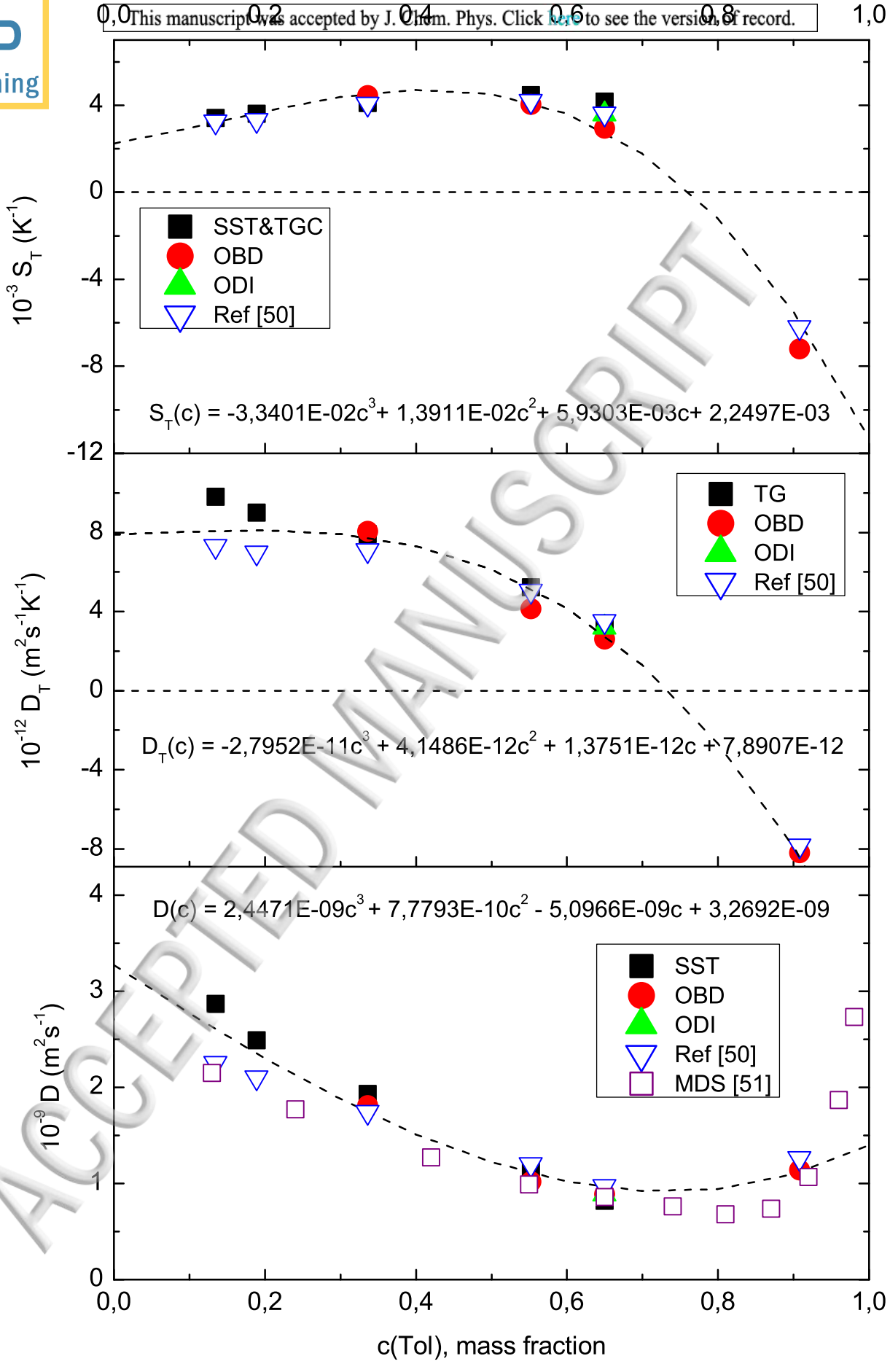

Tol-Ch binary mixture